4H-SiC Schottky diodes with Ni2Si contacts for X-ray detection

Article (Accepted Version)

4H-SiC Schottky diodes with Ni_2Si contacts for X-ray detection

G. Lioliou[1*], N.R. Gemmell[1], M. Mazzillo[2], A. Sciuto[3], A.M. Barnett[1]

[1] *Space Research Group, Sch. of Engineering and Informatics, University of Sussex, Falmer, Brighton, BN1 9QT, UK*

[2]*STMicroelectronics, Research and Development, Catania 95121, Italy*

[3]*National Research Council, Institute for Microelectronics and Microsystems, (CNR-IMM HQ) Catania 95121, Italy*

Abstract

4H-SiC Schottky photodiodes, with 25 μm epitaxial layers, employing thin (20 nm) Ni_2Si Schottky contacts, were investigated for high temperature photon counting X-ray spectroscopy. Important X-ray photodiode detector parameters were extracted from electrical characterization within the temperature range 160 °C to 0 °C. The devices were found to be fully depleted at an applied electric field of 20 kV/cm; a leakage current density of 33 nA cm^{-2} ± 1 nA cm^{-2} at 160 °C, was measured for one of the devices. The detectors were subsequently connected to low-noise photon counting readout electronics and investigated for their spectral performance at temperatures up to 100 °C. With the charge-sensitive preamplifier operated at the same temperature as the detector the best energy resolution (*Full Width at Half Maximum* at 5.9 keV) obtained decreased from 2.20 keV ± 0.04 keV (120 e^- rms ± 2 e^- rms) at 100 °C to 1.20 keV ± 0.03 keV (65 e^- rms ± 2 e^- rms) at 0 °C. The dominant source of noise broadening the ^{55}Fe X-ray photopeak was found to be the dielectric noise, except for the spectra accumulated at 100 °C and long shaping times (> 6 μs), in those case the main source of photopeak broadening was the white parallel noise.

Keywords: Silicon Carbide; 4H-SiC; Schottky diodes; X-ray spectroscopy.

1. Introduction

In recent years, the semiconductor material 4H-SiC has been considered for the development of radiation detectors due to its physical properties. Its wide bandgap, 3.26 eV [1], yields low thermally generated leakage currents, allowing high temperature operation. Its relatively low electron affinity, 3.17 eV [2], results in high Schottky barrier heights and hence in reduced thermionic emission current, which also contributes to high temperature operation. Another advantage of 4H-SiC radiation detectors is their short carrier transit times, i.e. incomplete charge collection noise can be minimised by application of high reverse electric fields due to the material's high breakdown field and high electron and hole saturation velocities [3]. Furthermore, 4H-SiC devices have been experimentally proven to be radiation hard [4]; the strong interatomic bonding in SiC and its correspondingly high displacement threshold energy (= 21.8 eV) [5] implies a longer lifetime for SiC detectors than Si detectors when operating in intense radiation environments.

In addition to X-ray detection, 4H-SiC radiation detectors have been investigated for UV [6], alpha particle [7], beta particle [8], neutron [9], light ion [10] [11] [12], and γ-ray [3] detection. The first reports of 4H-SiC spectroscopic X-ray detectors were with Au/4H-SiC Schottky diodes which had 30 μm n-type epitaxial layers [13]; a moderate energy resolution was achieved (electronic noise of 136 e^- r.m.s equivalent noise charge) under the illumination of an ^{241}Am γ-ray source. Development of prototype single pixel spectroscopic systems employing 4H-SiC epitaxial layers coupled to ultra-low noise electronics has resulted in near Fano-limited energy resolutions, the best energy resolutions (*FWHM* at 5.9 keV) reported to date are 196 eV at 30 °C and 233 eV at 100 °C; these were achieved using Au/4H-SiC Schottky diodes with 70 μm n-type epitaxial layers [14]. Development of NiSi/4H-SiC Schottky X-ray detectors has also been reported. Using a thin (18 nm) NiSi Schottky contact, X-ray attenuation within the contact is reduced, and hence the soft X-ray quantum detection efficiency is

* Corresponding author. Tel.: +44 (0) 1273 872568. E-mail address: G.Lioliou@sussex.ac.uk

improved, compared to using thicker Schottky contacts [15][16]. Such devices have been shown to perform spectroscopically with moderate energy resolutions at temperatures up to 80 °C and after proton irradiation, suggesting high temperature and radiation tolerance of the detectors. NiSi/4H-SiC Schottky X-ray detector arrays have also been reported; a *FWHM* at 17.4 keV of 1.36 keV, at a temperature of 30 °C was achieved with one such device [16].

An alternative to NiSi Schottky contacts on 4H-SiC Schottky diodes is Ni_2Si Schottky contacts; the higher metal work function of Ni_2Si (4.8 eV) compared to the metal work function of NiSi (4.5 eV) [17], may result in larger barrier height (i.e. reduced thermionic emission current) for Ni_2Si/4H-SiC Schottky diodes compared to that of NiSi/4H-SiC Schottky diodes. Ni_2Si/4H-SiC Schottky diodes have been investigated for alpha particle [18] [19], beta particle [20], and UV [6] detection.

In this paper, five thin (20 nm) metal film Ni_2Si/4H-SiC Schottky photodiodes are investigated for their suitability in high temperature (up to 100 °C) X-ray spectroscopy. The device fabrication is first described, then results from the electrical characterization (dark leakage current and capacitance) of the devices are presented and discussed. The saturation current, ideality factor, zero band barrier height, leakage current density, depletion width, and free carrier concentration, all within the temperature range 160 °C and 0 °C, are extracted from measurements. Two of the detectors, D1 and D2, were then coupled (in turn) to a custom-made charge-sensitive preamplifier and illuminated by an ^{55}Fe radioisotope X-ray source. ^{55}Fe X-ray spectra were first accumulated using both detectors at room temperature, and then from 100 °C to 0 °C using detector D2. The different noise contributions to the broadening of the photopeak were identified.

2. Device fabrication

The 4H-SiC Schottky diodes were fabricated at STMicroelectronics-Catania Research and Development facilities, Italy, in collaboration with CNR-IMM of Catania, Italy. The 4H-SiC wafer had a 25 μm thick n type (unintentional doping concentration < 10^{14} cm^{-3}) epitaxial layer grown on an n type substrate (300 μm thick with 10^{19} cm^{-3} doping concertation) by LPE - Italy. Sputter deposition of a 100 nm thick Ni film on the sample back side, followed by a rapid annealing at 1000 °C in N_2 ambient, resulted in the formation of 200 nm thick Ni_2Si contact layer, the Ohmic contact on the back side. Sputter deposition of a 10 nm thick Ni film on the sample front side, followed by a rapid annealing at 700 °C in N_2 ambient, resulted in the formation of ~ 20 nm thick Ni_2Si layer, the Schottky contact on the front side. The front metal contact was patterned through standard optical lithography and highly selective metal etch. The area of each fabricated device was 0.5 mm × 0.5 mm. The devices were planar and laterally defined by the front metal contact. The front bond pad consisted of an AlSiCu metallic layer.

3. Room temperature current measurements

The dark currents of all five diodes (D1-D5) as functions of forward and reverse applied bias were initially measured at room temperature. The diodes were in turn mounted in a light tight metal box enclosure; dry N_2 was continually flowing into the metal box to ensure a dry environment (< 5 % humidity). The bias was applied and the current was measured using a Keithley 6487 Picoammeter/Voltage Source [21]. The uncertainty associated with a single current measurement reading depended on the current range; for currents up to 2 nA, it was 0.3% of the measurement plus 0.4 pA.

The forward current, I_F, as a function of applied bias, V_{AF}, at room temperature can be seen in **Figure 1**. Identical forward current characteristics were measured for all five diodes. The effect of the series resistance, which resulted in the forward current deviating from an exponential rise, can be seen at

high applied forward biases ($\gtrsim$ 1 V) [22]. The saturation current, zero band barrier height, and the ideality factor of the Schottky diodes, were all extracted from the forward current measurements. The linear region of the logarithm of the forward current as a function of applied bias (ranging between the applied bias of 0.5 V and 0.9 V) was fitted using linear least squares fitting; the extrapolated value of the fitting to 0 V applied bias corresponded to the saturation current. It was found to be 2.0×10^{-19} A $\pm$ 0.2×10^{-19} A (rms deviance) for the five 4H-SiC Schottky diodes. The zero band barrier height was computed using the saturation current and assuming an effective Richardson constant of 146 A cm^{-2} K^{-2} [22] [23]; a value of 1.358 eV $\pm$ 0.003 eV (rms deviance) was calculated for the five 4H-SiC Schottky diodes, at room temperature. The Schottky barrier height ideally equals the difference between the metal work function (= 4.8 eV for Ni_2Si [17]) and the electron affinity of the semiconductor (= 3.17 eV for 4H-SiC [2]). Taking into account the effect of the series resistance, the ideality factor was computed from the $d(V_{AF})/d(I_F)$ as a function of I_F plot. An ideality factor value of 2.72 $\pm$ 0.02 (rms deviance) was calculated for the five 4H-SiC Schottky diodes, at room temperature. The difference between the ideal barrier height of Ni_2Si/4H-SiC (1.63 eV) and the measured value (1.358 eV), as well as the ideality factor's deviation from unity is discussed in the following section.

[Figure 1]

The leakage current, at up to -500 V reverse bias, was measured for each of the five 4H-SiC Schottky diodes at room temperature. The results can be seen in **Figure 2**. Similar leakage currents were measured for all five diodes. Applied reverse biases of -500 V created an applied electric field of 200 kV/cm across the depletion region (25 μm). Even at this high field strength, the leakage current remained $\leq$ 0.5 pA at room temperature, for all five diodes; a value of 0.14 pA $\pm$ 0.03 pA (rms deviance) and 0.33 pA $\pm$ 0.06 pA (rms deviance) at -200 V and at -500 V applied reverse bias was measured, respectively. It should be noted here that, even though the noise floor of the leakage current measuring system was $\pm$ 0.4 pA, **Figure 2** suggested that the uncertainty in leakage current decreased for a set of measurements not involving changes in temperature. Assuming no peripheral leakage current, the measured leakage current corresponded to a leakage current density of $\leq$ 200 pA cm^{-2} at the maximum applied reverse bias (200 kV/cm applied electric field), and $\leq$ 40 pA cm^{-2} at -250 V (100 kV/cm applied electric field). The lowest leakage current density at room temperature reported for a 4H-SiC Schottky diode was for Ni/4H-SiC diodes with a 115 μm epitaxial layer; a leakage current density of $\leq$ 10 pA cm^{-2} was reported at -200 V applied bias for that device [24]. Although anticipated to be negligible at room temperature, part of the measured leakage current may be attributed to packaging leakage current, hence the values presented in **Figure 2** represented the upper limit of the leakage currents of the 4H-SiC Schottky diodes.

[Figure 2]

4. Temperature dependence current measurements of D1

For two representative devices, D1 and D2, measurements were made of the temperature dependence of the device currents within the temperature range 160 °C to 0 °C. Each device was installed, in turn, in a light tight metal box enclosure inside a TAS LT climatic cabinet, for temperature control. The temperature was initially set to 160 °C, and gradually reduced to 0 °C, with a 20 °C step. Dry N_2 was continually flowing inside the climatic cabinet and the diode was left for 30 min at each temperature prior to measurements to mitigate any humidity effects (< 5 % humidity) and ensure thermal equilibrium. The bias was applied and the current was measured using a Keithley 6487 Picoammeter/Voltage Source [21]. The leakage currents associated with the devices' packaging was measured as a function of applied bias and temperature; it was then subtracted from the total measured leakage current of the packaged devices so that the characteristics of the devices themselves could be established.

The forward current as a function of applied bias of the 4H-SiC Schottky diode D1 can be seen in **Figure 3** at temperatures between 160 °C and 0 °C. The saturation current, zero band barrier height, and ideality factor, as functions of temperature were all extracted from the measurements. The saturation current decreased from 3.7×10^{-13} A ± 0.6×10^{-13} A at 160 °C to 4×10^{-21} A ± 2×10^{-21} A at 0 °C.

[Figure 3]

The computed zero band barrier height and ideality factor of D1, as a function of temperature can be seen in **Figure 4**. The zero band barrier height increased from 1.35 eV ± 0.01 eV at 0 °C to 1.485 eV ± 0.006 eV at 160 °C. The ideality factor improved from 2.88 ± 0.08 at 0 °C to 2.4 ± 0.1 at 160 °C. As the temperature decreased, from 160 °C to 0 °C, there was a bigger deviation from the ideal behaviour (i.e. ideality factor = 1), with the zero band barrier height to appearing to be lowered. The deviation from ideality observed at all temperatures, with an increased deviation at lower temperatures, suggested an inhomogeneous barrier [23]. The current through an inhomogeneous Schottky barrier may be expressed as the sum of currents flowing in an assortment of Schottky barrier height patches, with lower heights than that of an homogeneous barrier, as has been shown by Tung [25]. The current may be dominated by Schottky barrier height patches with lower height, as the temperature is decreased, leading to a larger ideality factor and lower apparent barrier height. In contrast, current transport across the metal-semiconductor interface at high temperatures may be dominated by electrons surmounting the higher barriers, resulting in an increase of the apparent barrier height. Similar non-idealities and barrier height dependencies on temperature have been reported for other 4H-SiC Schottky diodes [26] [27] [28]. The difference between the ideal barrier height of Ni_2Si/4H-SiC (1.63 eV) and the measured value (being temperature dependent and equal to 1.485 eV ± 0.006 eV at 160 °C), as well as the ideality factor deviating from unity, may be attributed to the presence of inhomogeneous barrier.

[Figure 4]

The temperature dependent measured leakage current as a function of applied reverse bias of the 4H-SiC Schottky diode D1 can be seen in **Figure 5**. Similar leakage currents were measured for diode D2. The leakage current of the 4H-SiC Schottky diode D1, at the maximum applied reverse bias, -200 V, was found to reduce from 0.97 nA ± 0.01 nA at 160 °C to 1.2 pA ± 0.6 pA at 80 °C, and to a value smaller than the uncertainty of the measuring system (± 0.4 pA) at temperatures < 80 °C. Similarly, the leakage current of the 4H-SiC Schottky diode D2, at the maximum applied reverse bias, -200 V, was found to reduce from 1.61 nA ± 0.02 nA at 160 °C to 2.7 pA ± 0.6 pA at 80 °C, and to a value smaller than the uncertainty of the measuring system (± 0.4 pA) at temperatures < 80 °C. Both the 4H-SiC Schottky diode detectors were reverse biased at -50 V for the X-ray spectroscopy measurements (see Section **6. ^{55}Fe X-ray spectroscopy**). The total (including package) leakage current at -50 V reverse bias was measured to be 6.4 pA ± 0.4 pA at 100 °C and ≤ 1 pA at temperatures ≤ 80 °C, and 6.3 pA ± 0.4 pA at 100 °C and ≤ 1 pA at temperatures ≤ 80 °C, for D1 and D2 respectively.

[Figure 5]

The leakage current density was calculated, assuming that there was no peripheral and/or surface leakage current, by simply dividing the 4H-SiC Schottky diode's leakage current by its total area. The leakage current density as calculated at three internal electric fields for the 4H-SiC Schottky diode D1 can be seen in **Figure 6**. Leakage current densities corresponding to leakage currents smaller than the uncertainty of the measuring system (≈ 4×10^{-13} A) were excluded from the figure.

The leakage current density of D1 was found to exponentially increase within the temperature range 100 °C (200 pA cm^{-2} ± 200 pA cm^{-2}) and 160 °C (33 nA cm^{-2} ± 1 nA cm^{-2}) for relatively low applied electric field strengths (= 20 kV/cm; -50 V applied bias). However, this was not the case for the leakage current density at 40 kV/cm and 80 kV/cm applied electric fields (see **Figure 6**). **Figure 6** suggested that the leakage current mechanism at high applied electric field strengths varied with temperature between 160 °C and 80 °C. In general, the diffusion current is less sensitive to temperature compared to the thermionic emission current; the tunnelling current becomes the dominant transport process at low temperatures, and Schottky-barrier lowering is the dominant effect when the generation current is small [22]. In addition to the above leakage current mechanisms, edge leakage current, arising from the edge around the periphery of the devices, may dominate the reverse current component for most practical Schottky diodes. Measuring the leakage current of devices with multiple diameters, to quantify the leakage current contribution (if any) of the contact periphery, and measuring the leakage current of unpackaged devices, to better and completely exclude the contribution of the package to the measured leakage current, would enable an improved understanding of the dominant leakage current mechanism as a function of temperature.

The high temperature leakage current densities of the currently reported Ni_2Si/4H-SiC Schottky diodes were lower, comparable, and higher than previously reported high quality GaAs, InGaP, and 4H-SiC diode detectors, respectively. For GaAs mesa p^+-i-n^+ photodiodes, typical leakage current densities of the order of ~ μA cm^{-2} (c.f. ~ nA cm^{-2} for D1) have been recorded at 100 °C when operated at an internal electric field of 50 kV/cm [29]. An $In_{0.5}Ga_{0.5}P$ mesa p^+-i-n^+ photodiode had ~ 1 pA leakage current at 100 °C when operated at an applied electric field of 30 kV/cm [30], similar to D1 (**Figure 5**). However, previously reported Au/4H-SiC Schottky diodes had leakage current densities of the order of 1 nA cm^{-2} at 100 °C and 103 kV/cm mean electric field [14], whereas 13 nA cm^{-2} at 100 °C and 80 kV/cm was measured for the presently reported Ni_2Si/4H-SiC Schottky diode D1.

[Figure 6]

5. Temperature dependence capacitance measurements of D1

The depletion layer width and the carrier concentration of the 4H-SiC Schottky diodes' epilayer within the temperature range 160 °C and 0 °C, were both determined from capacitance measurements. The packaged 4H-SiC Schottky diode D1 was installed in a light tight Al enclosure, inside a TAS Micro MT climatic cabinet for temperature control. The temperature was decreased from 160 °C to 0 °C, with a 20 °C step. Dry N_2 was continually flowing inside the climatic cabinet and the diode was left for 30 min at each temperature prior to measurements, to mitigate any humidity effects (< 5 % humidity) and ensure thermal equilibrium. The bias was applied using a Keithley 6487 Picoammeter/Voltage Source [21] and the capacitance was measured using an HP Multi Frequency LCR meter with a 50 mV rms magnitude and 1 MHz frequency test signal. The capacitance between an empty pin (adjacent to D1) and the package's common pin was measured and subtracted from the total measured capacitance of the packaged diode D1 to result in the Schottky diode's depletion layer capacitance. The uncertainty of the detector's capacitance, including the LCR meter accuracy, uncertainty arising from interconnections, and packaging capacitance uncertainty, was estimated to be ± 0.15 pF. It should be noted here that the reported capacitance variations with temperature, resulted from a single set of measurements taken at the same conditions (i.e., only the temperature was varied and no interconnections were changed), and hence, the associated uncertainty, including only the LCR meter accuracy and being proportional to the value of the corresponding measured capacitance, was estimated to range from ± 0.006 pF to ± 0.008 pF.

The 4H-SiC Schottky diode capacitance as a function of applied reverse bias within the temperature range 160 °C and 0 °C can be seen in **Figure 7**. The capacitance of D1 decreased as the reverse bias increased in magnitude from 0 V to -50 V; a reduction from (2.86 ± 0.15) pF at 0 V to (0.80 ± 0.15) pF at -50 V was recorded at 20 °C. No further decrease in capacitance was measured as the reverse bias further increased (in magnitude) beyond -50 V, suggesting that the epilayer of the Schottky diode was fully depleted. The depletion layer width of D1 was calculated from the measured depletion layer capacitance [22]. The depletion layer width was found to be temperature invariant within the investigated temperature range; values of 27.7 μm ± 0.2 μm and 27.3 μm ± 0.2 μm were calculated, at the maximum investigated reverse bias, at 160 °C and 0 °C respectively. The depletion layer width at 20 °C was measured to be 27 μm ± 5 μm, a value consistent with that provided by the epitaxial growth supplier (= 25 μm). The uncertainty of the calculated depletion layer width resulted from the propagation of the uncertainty in the capacitance measurements (± 0.15 pF).

[Figure 7]

The doping concentration in the epilayer was determined as a function of depletion layer width using the differential capacitance method [22], and can be seen in **Figure 8**, as calculated for 160 °C and 0 °C. The extracted doping concentration had a spatial resolution of the order of a Debye length, which has been calculated for 4H-SiC to be of the order of ≤ 0.2 μm, for the temperatures and doping densities of interest. The doping concentration was calculated; it varied between 3.4754×10^{13} cm^{-3} ± 0.0006×10^{13} cm^{-3} at 160 °C to 3.3638×10^{13} cm^{-3} ± 0.0007×10^{13} cm^{-3} at 0 °C, at the epilayer; a temperature invariant doping concentration, equal to 1×10^{16} cm^{-3} ± 1×10^{16} cm^{-3}, was calculated at the epilayer/substrate interface, within the temperature range 160 °C to 0 °C. The reported uncertainties were calculated by propagating the uncertainty associated with the capacitance measurements. The relatively low carrier concentration at the epilayer, similar to previously reported 4H-SiC Schottky diodes (= 6.48×10^{13} cm^{-3} [24]), as well as the abrupt change of the carrier concentration between the epilayer and the substrate, are both indicatives of the high quality of the devices.

[Figure 8]

6. ^{55}Fe X-ray spectroscopy

^{55}Fe X-ray spectra were accumulated using two of the 4H-SiC Schottky diode detectors, D1 and D2, to characterize their detection performance. An ^{55}Fe radioisotope X-ray source, with ≈ 140 MBq activity, was placed, in turn, 8 mm above each detector. Each detector, D1 and D2, was connected in turn to a custom-made single-channel charge sensitive preamplifier of a feedback resistorless design, similar to that described by ref. [31] and using a Si input JFET. The output signal of the preamplifier was shaped with an Ortec 572A shaping amplifier, which was further digitized using an Ortec EASYMCA 8k multi-channel analyser (MCA). ^{55}Fe X-ray spectra were initially obtained at room temperature; temperature dependent spectra, from 100 °C to 0 °C, were then obtained using the 4H-SiC Schottky diode D2. The preamplifier was operated at the same temperature as the photodiodes.

6.1. ^{55}Fe X-ray spectroscopy at room temperature with D1 and D2

Each X-ray spectrometer (4H-SiC detector coupled to the preamplifier and the back end electronics) was kept at room temperature. The operating reverse bias of both detectors during the ^{55}Fe X-ray spectra accumulation was chosen to be -50 V; the detectors' leakage current was negligible (<0.1 pA, **Figure 2**), their capacitance reached its minimum value and they were fully depleted (**Figure 7**) in this bias condition. The shaping time, τ, of the shaping amplifier was varied; spectra were accumulated for τ = 0.5 μs, 1 μs, 2 μs, 3 μs, 6 μs, and 10 μs. The live time of each spectrum was 60 s.

Due to the energy resolution of each spectrometer, the detected photopeak from the ^{55}Fe radioisotope X-ray source was the combination of the Mn Kα (5.9 keV) and Kβ (6.49 keV) emission lines [32]. Two Gaussians were fitted to each photopeak; the centroid channel number and the area under the Gaussian peak at 5.9 keV were the free parameters of the fit. The relative position of the centroid channel numbers and the relative areas of the two fitted Gaussians were kept fixed. The relative areas of the two Gaussian fits was calculated taking into account the appropriate emission ratio of the ^{55}Fe radioisotope X-ray source [33] and the relative quantum efficiency of the detectors at these two X-ray photon energies. The relative quantum efficiency of the detectors at 6.49 keV and 5.9 keV was 0.84; a quantum efficiency of 0.503 and 0.600 was calculated at 6.49 keV and 5.9 keV, respectively. The quantum detection efficiency at each photon energy was calculated as per ref. [34], using the linear X-ray absorption coefficient of SiC [35], assuming an absorption layer of 25 μm, and excluding the effect of the thin 20 nm thick Ni_2Si layer. An example ^{55}Fe X-ray spectrum obtained using D1, at τ = 3 μs, along with the fitted Gaussians, can be seen in **Figure 9**. The *FWHM* at 5.9 keV was measured for each spectrum.

[Figure 9]

Partial charge collection of charge created in the non-active layers of the detectors resulted in low energy tailing, which can also be seen in **Figure 9**. In order to quantify this partial charge collection, the valley-to-peak ratio (*V*/*P*) was calculated for all obtained spectra, from the ratio between counts at the valley (channel number corresponding to 3.5 keV) and counts at the peak (centroid channel number of the 5.9 keV peak). It was found to be 0.05 for both 4H-SiC Schottky diode detectors, at -50 V reverse bias and room temperature. The counts of the zero energy noise peak were eliminated by setting the MCA low energy cut-off at ≈ 2 keV. However, a small portion of the zero energy noise peak can still be seen in **Figure 9**. The *FWHM* at 5.9 keV using both 4H-SiC Schottky diodes, as a function of shaping time, at -50 V reverse bias and room temperature can be seen in **Figure 10**.

[Figure 10]

The optimum shaping time used was found to be 3 μs and 2 μs for D1 and D2, respectively, with a *FWHM* at 5.9 keV of 1.29 keV ± 0.03 keV (70 e^- rms ± 2 e^- rms ENC). The estimated uncertainty of the reported *FWHM* at 5.9 keV values was related to the fitting of the Gaussians to the ^{55}Fe X-ray photopeaks. The energy resolution (*FWHM* at 5.9 keV) of both spectrometers as a function of shaping time was used to analyse the noise of each system and identify the dominant noise contribution to the broadening of the photopeak. The quadratic sum of three independent noises categories defines the energy resolution of a non-avalanche photodiode based spectrometer [36]. These are the Fano noise, the incomplete charge collection (incomplete CC) noise, and the electronic noise. The electronic noise consists of the white parallel noise (*WP*), the white series noise (*WS*) (including the induced gate current noise), the 1/*f* noise, and the dielectric noise. For a detailed description of the different noise components, the reader is referred to refs [36] [37].

All the above noise components are shaping time invariant, apart from the white series noise and the white parallel noise. The white series noise is inversely proportional to the shaping time and it arises from the total capacitance at the input of the preamplifier. The white parallel noise is directly proportional to the shaping time and it arises from the total leakage current flowing at the detector and preamplifier's input JFET. Hence, a multidimensional least squares fitting estimation method can be applied to the experimental values of the *FWHM* at 5.9 keV as a function of shaping time to detangle the differently shaping time dependent noise contributions (i.e. those that are proportional to shaping time, inversely proportional to shaping time, and shaping time invariant). This can be seen in **Figure 11**.

[Figure 11]

The dominant source of noise, within the investigated shaping time range (0.5 μs to 10 μs) was found to be the quadratic sum of Fano noise, 1/*f* noise, dielectric noise, and incomplete charge collection noise. This sum was estimated to be similar for both spectrometers employing the 4H-SiC Schottky diodes; it was found to be 65 e^- rms ± 1 e^- rms for D1 and 67 e^- rms ± 1 e^- rms for D2. The total leakage current of each spectrometer, including twice the contribution of the detector leakage current and the input JFET leakage current (the detector leakage current, which flows in the Drain-to-Source junction, and the Drain-to-Source junction current, are considered as two statistically independent components, due to the total capacitance at the input of the preamplifier [31]; the same applies for the input JFET leakage current), was estimated from the shaping time proportional contribution of the multidimensional least squares fitting of the measured *FWHM* at 5.9 keV as a function of shaping time (**Figure 11**), and was found to be 12 pA ± 1 pA and 6 pA ± 2 pA, when D1 and D2 were used, respectively. Similarly, the total capacitance of each spectrometer was estimated from the shaping time inversely proportional contribution seen in **Figure 11**; it was found to equal 3.8 pF ± 0.1 pF and 3.1 pF ± 0.3 pF, when D1 and D2 were used, respectively. The small differences between the total leakage current and capacitance being present in the X-ray spectrometers were attributed to the preamplifier's input JFET being slightly differently biased when each 4H-SiC Schottky diode was connected. The uncertainties of the extracted quadratic sum of Fano noise, 1/*f* noise, dielectric noise, and incomplete charge collection noise, total leakage current, and total capacitance of each spectrometer were related to the goodness of the multidimensional least squares fitting.

6.2. Temperature dependence ^{55}Fe X-ray spectroscopy with D2

^{55}Fe X-ray spectra were obtained as a function of temperature, within the temperature range 100 °C and 0 °C. The Si input JFET of the preamplifier prevented use of the system at temperatures > 100 °C. The 4H-SiC Schottky diode detector, D2, was coupled to a custom-made single-channel charge sensitive preamplifier, and the detector/preamplifier system was kept inside a TAS Micro LT climatic cabinet for temperature control. The temperature was initially set to 100 °C and decreased to 0 °C, in 20 °C steps, while dry N_2 was continually flowing in the climatic cabinet to ensure dry environment throughout the measurements, and mitigating humidity related effects. The applied reverse bias to the detector was chosen to be -50 V, as was the case for the room temperature ^{55}Fe X-ray spectra. At each temperature ^{55}Fe spectra were accumulated as functions of shaping time. However, at 100 °C, the longest shaping time used was 2 μs due to the large *FWHM* at 5.9 keV (> 2.3 keV) for shaping times ≥ 3 μs. The live time of each spectrum was 60 s. Gaussians were fitted to the ^{55}Fe X-ray photopeaks of the obtained spectra, and the *FWHM* at 5.9 keV of each was recorded. The obtained spectra with the best energy resolution (*FWHM* at 5.9 keV) at 100 °C and 0 °C, for the spectrometer employing the 4H-SiC Schottky diode, D2, can be seen in **Figure 12**.

[Figure 12]

The low energy tailing, seen in **Figure 12**, resulted from partial charge collection of charge created in the non-active layers of the device. In addition to partial charge collection, the zero energy noise peak overlapped the ^{55}Fe photopeak at high temperatures (i.e. 100 °C, see **Figure 12 (a)**), which resulted in further increase of the valley-to-peak ratio. The *V*/*P* ratio, defined as the ratio between counts at the valley (channel number corresponding to 3.5 keV, apart from spectra at 100 °C, where the valley was at a channel number corresponding to 4.2 keV) and counts at the peak (centroid channel number of the 5.9 keV peak) was calculated; it improved from 0.44 ± 0.02 at 100 °C (-50 V reverse bias and 1 μs shaping time), to 0.052 ± 0.008 at 0 °C (-50 V reverse bias and 10 μs shaping time) and it broadly followed the improvement of the *FWHM* at 5.9 keV. The uncertainties associated to the *V*/*P* ratio were calculated assuming a Poissonian process; the statistical fluctuation of the total number of the

detected counts in each channel equalled the square root of the total number of counts within the channel. The best energy resolution (*FWHM*) at 5.9 keV improved from 2.20 keV ± 0.04 keV (120 e^- rms ± 2 e^- rms) at 100 °C to 1.20 keV ± 0.03 keV (65 e^- rms ± 2 e^- rms) at 0 °C. The best *FWHM* at 5.9 keV at each temperature can be seen in **Figure 13**. It should be noted here that the *FWHM* at 5.9 keV, at 0 °C, remained stable from 2 μs (1.21 keV ± 0.03 keV) to 10 μs (1.20 keV ± 0.03 keV), within uncertainties.

[Figure 13]

There was a bigger improvement in *FWHM* at 5.9 keV as the temperature decreased from 100 °C to 80 °C, compared to the same improvement as the temperature decreased from 20 °C to 0 °C. The best obtained *FWHM* at 5.9 keV improved by 360 eV ± 50 eV for a 20 °C temperature reduction, from 2.20 keV ± 0.04 keV at 100 °C to 1.83 ± 0.03 keV at 80 °C, whereas there was only 60 eV ± 40 eV reduction in the best obtained *FWHM* at 5.9 keV for a 20 °C temperature reduction, from 1.26 keV ± 0.03 keV at 20 °C to 1.20 ± 0.03 keV at 0 °C. In order to explain this observation and detangle the three noise contributions (proportional to shaping time, inversely proportional to shaping time, and shaping time invariant) at each temperature, a multidimensional least squares fitting estimation method was used to the experimental values of the *FWHM* at 5.9 keV as a function of shaping time, within the temperature range 100 °C to 0 °C, and it can be seen in **Figure 14**.

[Figure 14]

The dominant source of noise within the investigated shaping time and temperature range was the quadratic sum of the dielectric noise, incomplete charge collection noise, 1/*f* noise, and Fano noise, apart from at shaping times > 6 μs and a temperature of 100 °C (both conditions fulfilled), where the white parallel noise dominated.

The 1/*f* noise can be calculated as per ref. [36] and the Fano noise as per ref. [38]. The 1/*f* noise was calculated to reduce from 96 eV at 100 °C, to 73 eV at 0 °C, for the detector reverse biased at -50 V. The Fano noise was calculated to be equivalent to 160 eV at 5.9 keV, assuming a Fano factor of F = 0.1 [14] and an electron hole pair creation energy of ω = 7.8 eV [39]. Subtracting in quadrature the 1/*f* and the Fano noise from the shaping time invariant noise contribution, and assuming insignificant incomplete charge collection noise, the result is the dielectric noise contribution, which can be seen in **Figure 15 (a)**. The dielectric noise of the X-ray spectroscopic system based on the 4H-SiC Schottky diode D1 reduced from 1.90 keV (equivalent to 103 e^- rms) at 100 °C to 1.10 keV ± 0.03 keV (equivalent to 61 e^- rms ± 2 e^- rms) at 0 °C. The uncertainties of the dielectric noise contribution resulted from the uncertainties of the extracted quadratic sum of Fano noise, 1/*f* noise, dielectric noise, and incomplete charge collection noise, which were related to the goodness of the multidimensional least squares fitting, and assuming negligible uncertainty in the calculated Fano and 1/*f* noise. The uncertainty of the dielectric noise contribution at 100 °C could not be calculated, since the multidimensional fitting performed to only three experimental values of the *FWHM* at 5.9 keV (at 0.5 μs, 1 μs, and 2 μs), number equal to the number of coefficients of the multidimensional fit. The dielectric noise depends proportionally on the temperature [36] and hence, a reduction of the dielectric noise with reduced temperature was expected. The temperature effect on the dielectric noise is not only limited to this dependence; the dielectric noise depends on the capacitance and the dissipation factor of the lossy dielectrics, which may also be temperature dependent. The dielectric noise was attributed to lossy dielectrics at the input of the preamplifier, including the JFET's dielectrics, passivation, and packaging, the feedback capacitance, the detector's packaging, and the detector itself [37] [39] [40].

The white series noise contribution was found to decrease with decreased temperature for the reported spectrometer. The deduced total capacitance at the input of the preamplifier, giving rise to white series noise, can be seen in **Figure 15 (b)**. It was found to be 4.9 pF at 100 °C, reducing to 3.7 pF ± 0.3 pF at 0 °C; the total capacitance was temperature invariant from 80 °C to 0 °C, within uncertainties. The uncertainties of the extracted total capacitance of the X-ray spectrometer were related to the goodness of the multidimensional least squares fitting; the uncertainty of the total capacitance at 100 °C could not be calculated, since the multidimensional fitting at 100 °C performed to only three experimental values of the *FWHM* at 5.9 keV. The reduction of the total capacitance as the temperature decreased from 100 °C to 0 °C was attributed to the reduction of the input JFET capacitance, since the detector capacitance at -50 V reverse bias was temperature invariant (**Figure 6**). The input JFET capacitance may vary with temperature due to the change of the bias condition of the input JFET.

Similarly to the white series noise contribution, the white parallel noise was also found to decrease with decreased temperature. The total leakage current giving rise to the observed white parallel noise can be seen in **Figure 15 (c)**, as a function of temperature. It was found to reduce from 134 pA at 100 °C to 4 pA ± 2 pA at 0 °C. The uncertainties of the extracted total leakage current of the X-ray spectrometer were related to the goodness of the multidimensional least squares fitting; the uncertainty of the total leakage current at 100 °C could not be calculated, since the multidimensional fitting at 100 °C performed to only three experimental values of the *FWHM* at 5.9 keV. Since the deduced total leakage current consisted of twice the contribution of the detector's and the input JFET's leakage current [31], it can be said that the sum of the detector's and the input JFET's leakage current, including their package leakage current, reduced from 67 pA at 100 °C to 2 pA ± 1 pA at 0 °C. At -50 V reverse bias, the total leakage current of D2 was measured to be 6.3 pA ± 0.4 pA at 100 °C, and ≤ 1 pA at ≤ 80 °C. Hence, the leakage current of the input Si JFET, along with its package, dominated over the 4H-SiC detector's leakage current, which emphasizes the importance of ultra-low-noise preamplifier electronics.

[Figure 15]

The energy resolution (*FWHM* at 5.9 keV) of the X-ray spectrometer employing D2 (e.g. 1.26 keV at 20 °C) is better than previously reported semi-transparent 4H-SiC Schottky diodes (1.49 keV at 5.9 keV [41] and 1.36 at 22.16 keV [15]) and better than commercial 4H-SiC Schottky UV photodiodes repurposed for X-ray detection (1.8 keV at 5.9 keV [42]). However, the best energy resolution achieved with a 4H-SiC X-ray detector was far better than the currently reported results; 0.233 keV *FWHM* at 5.9 keV at 100 °C was reported using an ultra high quality 4H-SiC Schottky diode coupled to ultra-low-noise electronics (8.9 e^- rms electronic noise) [14]. It should be noted here that 103 e^- rms out of 120 e^- rms (= *ENC* at 5.9 keV, at 100 °C), was the dielectric noise of the X-ray spectroscopic system. The dielectric noise contribution of the detector and the input JFET was calculated as per ref. [36], assuming a dissipation factor of 4×10^{-4} for 4H-SiC [43] and 2×10^{-3} for Si [44]; it was calculated to be 24 e^- rms for the 4H-SiC detector, 39 e^- rms for the input JFET, and 46 e^- rms their combined contribution. If the stray dielectric noises (i.e. dielectric noises other than those of the detector and JFET themselves) could be eliminated by an improved design of the preamplifier's input, 45 e^- rms out of the 64 e^- rms total dielectric noise (since 46 e^- rms corresponded to the combined contribution of the detector and input JFET dielectric noise) would be eliminated and the achievable energy resolution would improve to 0.95 keV at 5.9 keV, at 20 °C. This result emphasizes the need for the development of low noise electronics, specifically designed to be used with wide bandgap semiconductor detectors, whose relatively larger electron hole pair creation energy results in relatively poorer energy resolution for a given *ENC*, compared to narrow bandgap semiconductor detectors.

The operation of the X-ray spectrometer at temperatures > 100 °C was limited by the electronic noise of the preamplifier electronics, rather than the 4H-SiC Schottky photodiode detector itself. The capacitance of the detector was found to be temperature invariant within the temperature range 100 °C and 160 °C, implying that the white series noise and the 1/*f* noise contributions (both capacitance dependent) from the detector would not increase for a temperature increase from 100 °C to 160 °C. Also, the leakage current of the 4H-SiC Schottky photodiode at -50 V applied reverse bias (excluding the leakage current of the package), was found to increase from 0.3 pA ± 0.6 pA at 100 °C to 33 pA ± 4 pA at 160 °C, suggesting a small increase of the white parallel noise contribution of the detector from 2 e^- rms at 100 °C to 20 e^- rms at 160 °C (at 1 μs shaping time). The dielectric noise contribution of the 4H-SiC Schottky photodiode detector would be expected to increase as the temperature increases from 100 °C to 160 °C, given that it is directly proportional to the temperature. However, the temperature invariant capacitance of the reported detector, along with the relatively small value of the dissipation factor of 4H-SiC (of the range of 10^{-4} at 22 °C, at 40 GHz [43]) suggested a relatively small increase of the dielectric noise contribution of the 4H-SiC Schottky photodiode detector for a temperature increase from 100 °C to 160 °C.

7. Conclusions

For the first time, 4H-SiC Schottky photodiodes employing thin (20 nm) Ni_2Si Schottky contacts were evaluated for high temperature photon counting X-ray spectroscopy. Electrical characterization of the devices at temperatures from 160 °C to 0 °C was followed by ^{55}Fe X-ray spectra measurements using two devices at room temperature, and one device at temperatures from 100 °C to 0 °C.

Detector current measurements as functions of applied bias at room temperature were similar for all five 4H-SiC Schottky diodes. The devices exhibited low leakage current densities (≤ 200 pA cm^{-2} at an applied electric field of 200 kV/cm and room temperature), a zero band barrier height (1.358 eV ± 0.003 eV) smaller than expected (1.63 eV), and an ideality factor (2.72 ± 0.02) which deviated from unity. The presence of an inhomogeneous barrier was suggested from temperature dependent current measurements. Leakage currents at -200 V applied reverse bias of 0.97 nA ± 0.01 nA and 1.61 nA ± 0.02 nA at 160 °C were measured for D1 and D2, respectively. Both devices had leakage currents smaller than the uncertainty of the measuring system for temperatures < 80 °C. Capacitance measurements suggested that the devices were fully depleted at -50 V applied bias, with a calculated depletion layer width (temperature invariant) of 27 μm ± 5 μm. A temperature invariant doping concentration was also extracted; it varied from 3×10^{13} cm^{-3} at the epilayer to 1×10^{16} at the epilayer-substrate interface within the temperature range 160 °C to 0 °C.

The best energy resolution (*FWHM* at 5.9 keV) achieved at room temperature was 1.29 keV ± 0.03 keV (70 e^- rms ± 2 e^- rms ENC) with detector D2. The dominant source of noise, within the investigated shaping time range (0.5 μs to 10 μs) was found to be the quadratic sum of Fano noise, 1/*f* noise, dielectric noise, and incomplete charge collection noise. ^{55}Fe X-ray spectra obtained using D2 had a *FWHM* at 5.9 keV of 2.20 keV ± 0.04 keV (120 e^- rms ± 2 e^- rms) at 100 °C, which improved to 1.20 keV ± 0.03 keV (65 e^- rms ± 2 e^- rms) at 0 °C. Noise analysis of the spectroscopic system revealed that the dominant source of noise was the dielectric noise, within the temperature and shaping time ranges investigated, apart from > 6 μs and 100 °C where the white parallel noise dominated. The dielectric noise of the X-ray spectroscopic system based on the 4H-SiC Schottky diode D2 was found to reduce from 1.90 keV (equivalent to 103 e^- rms) at 100 °C to 1.10 keV ± 0.03 keV (equivalent to 61 e^- rms ± 2 e^- rms) at 0 °C.

The reported X-ray spectrometer based on Ni_2Si/4H-SiC Schottky diode detectors had a modest energy resolution compared to the best achieved with 4H-SiC X-ray detectors, but its energy resolution was limited by the preamplifier electronics rather than the detector itself. The results

indicate that little energy resolution degradation would be expected as a consequence of the detector itself if the operating temperature was increased from 100 °C to 160 °C; rather the preamplifier is the limiting factor in this condition. All the above results, along with previously reported 4H-SiC radiation hardness measurements, suggested that the Ni_2Si/4H-SiC Schottky diode detectors may find uses in future applications for X-ray detection in environments of high temperature and intense radiation.

ACKNOWLEDGEMENTS

This work was in part supported by the Engineering and Physical Sciences Research Council, United Kingdom, through grant EP/P021271/1 (A.M.B., PI). A.M.B. acknowledges funding from the Leverhulme Trust, United Kingdom, in the form of a 2016 Philip Leverhulme Prize.

Data underlying this work are subject to commercially confidentiality. The Authors regret that they cannot grant public requests for further access to any data produced during the study.

REFERENCES

[1] G. L. Harris, Properties of Silicon Carbide, Institution of Electrical Engineers London; 1995.
[2] S. Yu. Davydov, *Semiconductors* **41**, 2007, 696.
[3] G. Bertuccio, D. Puglisi, A. Pullia and C. Lanziery, *IEEE Transactions on Nuclear Science* **60**, 2013, 1436.
[4] F. Nava, E. Vittone, P. Vanni, G. Verzellesi, P. G. Fuochi, C. Lanzieri, and M. Glaser, *Nuclear Instruments and Methods in Physics Research A* **505**, 2003, 645.
[5] A. Owens, Compound Semiconductor Radiation Detectors, CRC Press Florida; 2012.
[6] A. Sciuto, M. Mazzillo, P. Badala, M. Scuderi, B. Carbone, and S. Coffa, *IEEE Photonics Technology Letters* **26**, 2014, 1782.
[7] F. H. Ruddy, J. G. Seidel, H. Chen, A.R. Dulloo, and S. H. Ryu, *IEEE Transactions on Nuclear Science* **53**, 2006, 1713.
[8] F. Nava, P. Vanni, M. Bruzzi, S. Lagomarsino, S. Sciortino, G. Wagner, and C. Lanzieri, *IEEE Transactions on Nuclear Science* **51**, 2004, 238.
[9] F. H. Ruddy, A. R. Dulloo, J.G. Seidel, M. K. Das, S. H. Ryu, and A. K. Agarwal, *IEEE Transactions on Nuclear Science* **53**, 2006, 1666.
[10] M. De Napoli, G. Raciti, E. Rapisarda, and C. Sfienti, *Nuclear Instruments and Methods in Physics Research A* **572**, 2007, 831.
[11] M. De Napoli, F. Giacoppo, G. Raciti, and E. Rapisarda, *Nuclear Instruments and Methods in Physics Research A* **608**, 2009, 80.
[12] M. De Napoli, F. Giacoppo, G. Raciti, and E. Rapisarda, *Nuclear Instruments and Methods in Physics Research A* **600**, 2009, 618.
[13] G. Bertuccio, R. Casiraghi and F. Nava, *IEEE Transactions on Nuclear Science* **48**, 2001, 232.
[14] G. Bertuccio, S. Caccia, D. Puglisi, and D. Macera, *Nuclear Instruments and Methods in Physics Research Section A* **652**, 2011, 193.
[15] J. E. Lees, A. M. Barnett, D. J. Bassford, R. C. Stevens and A. B. Horsfall, *Journal of Instrumentation* **6**, 2011, C01032.
[16] G. Lioliou, H. K. Chan, T. Gohil, K. V. Vassilevski, N. G. Wright, A. B. Horsfall, and A. M. Barnett, *Nuclear Instruments and Methods in Physics Research A* **840**, 2016, 145.
[17] J. A. Kittl, M. A. Pawlak, A. Lauwers, C. Demeurisse, K. Opsomer, K. G. Anil, C. Vrancken, M. J. H. van Dal, A. Veloso, S. Kubicek, P. Absil, K. Maex, and S. Biesemans, *IEEE Electron Device Letters* **27**, 2006, 34.
[18] F. Nava, G. Wagner, C. Lanzieri, P. Vanni, and E. Vittone, *Nuclear Instruments and Methods in Physics Research A* **510**, 2003, 273.
[19] L. Torrisi, A. Sciuto, A. Cannavò, S. Di Franco, M. Mazzillo, P. Badalà, and L. Calcagno, *Journal of Electronic materials* **46**, 2017, 4242.

[20] S. Sciortino, F. Hartjes, S. Lagomarsino, F. Nava, M. Brianzi, V. Cindro, C. Lanzieri, M. Moll, and P. Vanni, *Nuclear Instruments and Methods in Physics Research A* **552**, 2005, 138.
[21] Keithley Instruments, Model 6487 Picoammeter/Voltage Source Reference Manual, 6487-901-01 Rev C, Keithley Instruments Inc. Ohio; 2011.
[22] S. M. Sze and K. K. Ng. 3rd ed., Physics of Semiconductor Devices. John Wiley & Sons New Jersey; 2007.
[23] F. Roccaforte, F. La Via, V. Raineri, R. Pierobon, and E. Zanoni, *Journal of Applied Physics* **93**, 2003, 9137.
[24] G. Bertuccio, D. Puglisi, D. Macera, R. Di Liberto, M. Lamborizio, and L. Mantovani, *IEEE Transactions on Nuclear Science* **61**, 2014, 961.
[25] R.T. Tung, *Applied Physics Letters* **58**, 1991, 2821.
[26] B. J. Skromme, E. Luckowski, K. Moore, M. Bhatnagar, C. E. Weitzel, T. Gehoski, and D. Ganser, *Journal of Electronic Materials* **29**, 2000, 376.
[27] L. Calcagno, A. Ruggiero, F. Roccaforte, and F. La Via, *Journal of Applied Physics* **98**, 2005, 023713.
[28] S. Qing-Wen, Z. Yu-Ming, Z. Yi-Men, C. Feng-Ping, and T. Xiao-Yan, *Chinese Physics B* **20**, 2011, 057301.
[29] G. Lioliou, M. D. C. Whitaker, and A. M. Barnett, *Journal of Applied Physics* **122**, 2017, 244506.
[30] S. Butera, G. Lioliou, A. B. Krysa, and A. M. Barnett, *Nuclear Instruments and Methods in Physics Research A* **908**, 2018, 277.
[31] G. Bertuccio, and A. Pullia, *Review of Scientific Instruments* **64**, 1993, 3294.
[32] U. Schötzig, *Applied Radiation and Isotopes* **53**, 2000, 469.
[33] M. Sánchez del Rio, A. Brunetti, B. Golosio, A. Somogyi, and A. Simionovici, A., XRAYLIB Tables (X-ray Fluorescence Cross-Section), European Synchrotron Radiation Facility and University of Sassari; 2003.
[34] G.W. Fraser, X-ray Detectors in Astronomy. Cambridge University Press Cambridge; 1989.
[35] J.H. Hubbell, *The International Journal of Applied Radiation and Isotopes* **33**, 1982, 1269.
[36] G. Lioliou, and A. M. Barnett, *Nuclear Instruments and Methods in Physics Research A* **801**, 2015, 63.
[37] G. Bertuccio, A. Pullia, and G. De Geronimo, *Nuclear Instruments and Methods in Physics Research Section A* **380**, 1996, 301.
[38] G. Bertuccio, *IEEE Solid-State Circuits Magazine* **4**, 2012, 36.
[39] G. Bertuccio, and R. Casiraghi, *IEEE Transactions on Nuclear Science* **50**, 2003, 175.
[40] G. Bertuccio, and A. Pullia, *Review of Scientific Instruments* **64**, 1993, 3294.
[41] J. E. Lees, D. J. Bassford, G. W. Fraser, A. B. Horsfall, K. V. Vassilevski, N. G. Wright and A. Owens, *Nuclear Instruments and Methods in Physics Research Section A* **578**, 2007, 226.
[42] S. Zhao, T. Gohil, G. Lioliou, and A. M. Barnett, *Nuclear Instruments and Methods in Physics Research A* **830**, 2016, 1.
[43] J. G. Hartnett, D. Mouneyrac, J. Krupka, J. M. le Floch, M. E. Tobar, and D. Cros, *Journal of Applied Physics* **109**, 2011, 064107.
[44] H. S. Jung, W. I. Yang, M. S. Cho, K. N. Joo, and S. Y. Lee, *Electronic Materials Letters* **10**, 2014, 541.

Figure 1. Current as a function of forward bias of the 4H-SiC Schottky diode, D1 (- symbols), D2 (filled circles), D3 (open squares), D4 (+ symbols), and D5 (filled diamonds), at room temperature.
Figure 2. Leakage current as a function of reverse bias of the 4H-SiC Schottky diode, D1 (- symbols), D2 (filled circles), D3 (open squares), D4 (+ symbols), and D5 (filled diamonds), at room temperature.
Figure 3. Current as a function of forward bias of the 4H-SiC Schottky diode, D1, within the temperature range 160 °C to 0 °C.
Figure 4. Calculated (a) zero band barrier height and (b) ideality factor of the 4H-SiC Schottky diode, D1, as a function of temperature.
Figure 5. Dark current as a function of reverse bias of the 4H-SiC Schottky diode, D1, within the temperature range 160 °C to 80 °C. The dark current was measured to be smaller than the uncertainty of the measuring system at temperatures < 80 °C.
Figure 6. Leakage current density as a function of temperature at three electric fields, 80 kV/cm (-200 V applied reverse bias) (filled circles), 40 kV/cm (-100 V applied reverse bias) (open diamonds), and 20 kV/cm (-50 V applied reverse bias) (× symbol), of the 4H-SiC Schottky diode, D1. Lines are guides for the eye only.
Figure 7. (a) Capacitance and (b) calculated depletion layer width as a function of reverse bias of the 4H-SiC Schottky diode, D1, at 160 °C (dashed line) and 0 °C (solid line). The error bars for the depletion layer width at 0 °C, as calculated based on the uncertainties in the capacitance measurements, can also be seen.
Figure 8. Calculated effective carrier concentration of the 4H-SiC Schottky diode, D1, at 160 °C (dashed line) and 0 °C (solid line).
Figure 9. The ^{55}Fe X-ray photopeak as obtained using the 4H-SiC Schottky diode, D1, at -50 V reverse bias and 3 μs shaping time. The individually fitted Mn Kα (5.9 keV) and Mn Kβ (6.49 keV) Gaussian peaks, along with their combination, are also shown.
Figure 10. *FWHM* of the 5.9 keV peak, using the 4H-SiC Schottky diode D1 (circles) and D2 (diamonds), as a function of shaping time, at -50 V reverse bias. The ENC (in e^- rms) is also shown.
Figure 11. Equivalent noise charge at 5.9 keV for the 4H-SiC Schottky diode (a) D1 and (b) D2 as a function of shaping time. The three noise contributions, inversely proportional to shaping time (white series), directly proportional to shaping time (white parallel) and shaping time invariant (Fano, 1/*f*, dielectric, and incomplete charge collection) have been determined with a multidimensional least squares fitting of the experimental points. The error bars were smaller than the symbols' size, and thus were omitted.
Figure 12. ^{55}Fe X-ray spectra accumulated with the 4H-SiC Schottky diode, D2, at (a) 100 °C (-50 V reverse bias and 1 μs shaping time) and (b) 0 °C (-50 V reverse bias and 10 μs shaping time). The fitted Mn Kα (5.9 keV) and Mn Kβ (6.49 keV) Gaussian peaks, along with their combination, can also be seen.
Figure 13. *FWHM* at 5.9 keV (using the 4H-SiC Schottky diode, D2) as a function of temperature, at -50 V reverse bias. The ENC (in e^- rms), and the optimum shaping time [μs] at each temperature is also shown.
Figure 14. *FWHM* at 5.9 keV (using the 4H-SiC Schottky diode, D2) as a function of shaping time, at -50 V reverse bias, within the investigated temperature range, 100 °C to 0 °C. The solid lines show the multidimensional least squares fitting to the experimental *FWHM* at 5.9 keV. The error bars were smaller than the symbols' size, and thus were omitted.
Figure 15. (a) Total dielectric noise (assuming negligible contribution from incomplete charge collection noise), (b) capacitance contribution to the white series noise, and (c) total leakage current contribution to the white parallel noise for the spectrometer employing 4H-SiC Schottky diode, D2, and as deduced from the multidimensional least squares fitting of the measured *FWHM* at 5.9 keV as a function of shaping time at -50 V reverse bias, at each temperature.

Figure 1

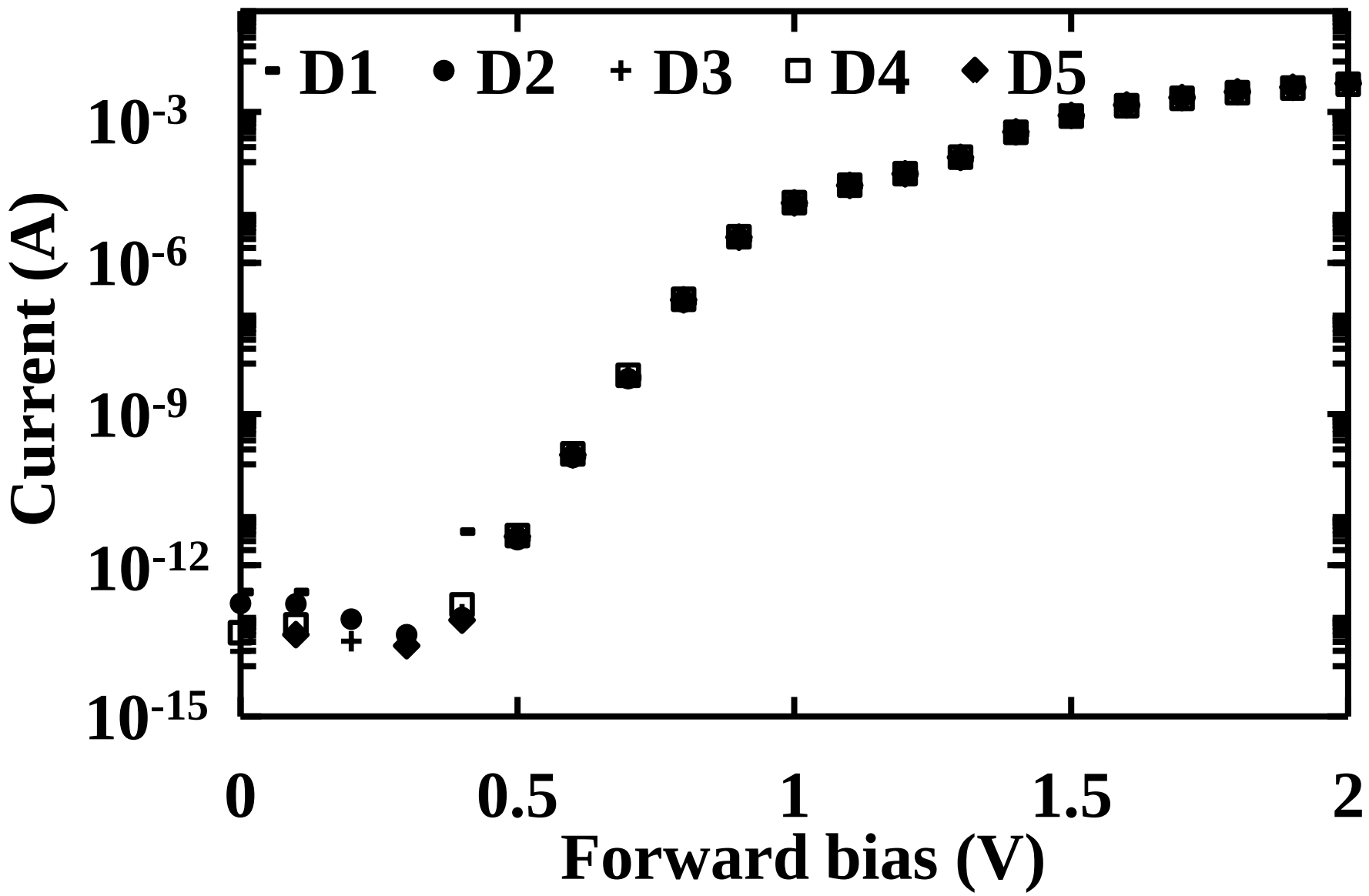
D1
D2
D3
D4
D5
Current (A)
10-3
10-6
10-9
10-12
10-15
0
0.5
1
1.5
2
Forward bias (V)

Figure 2

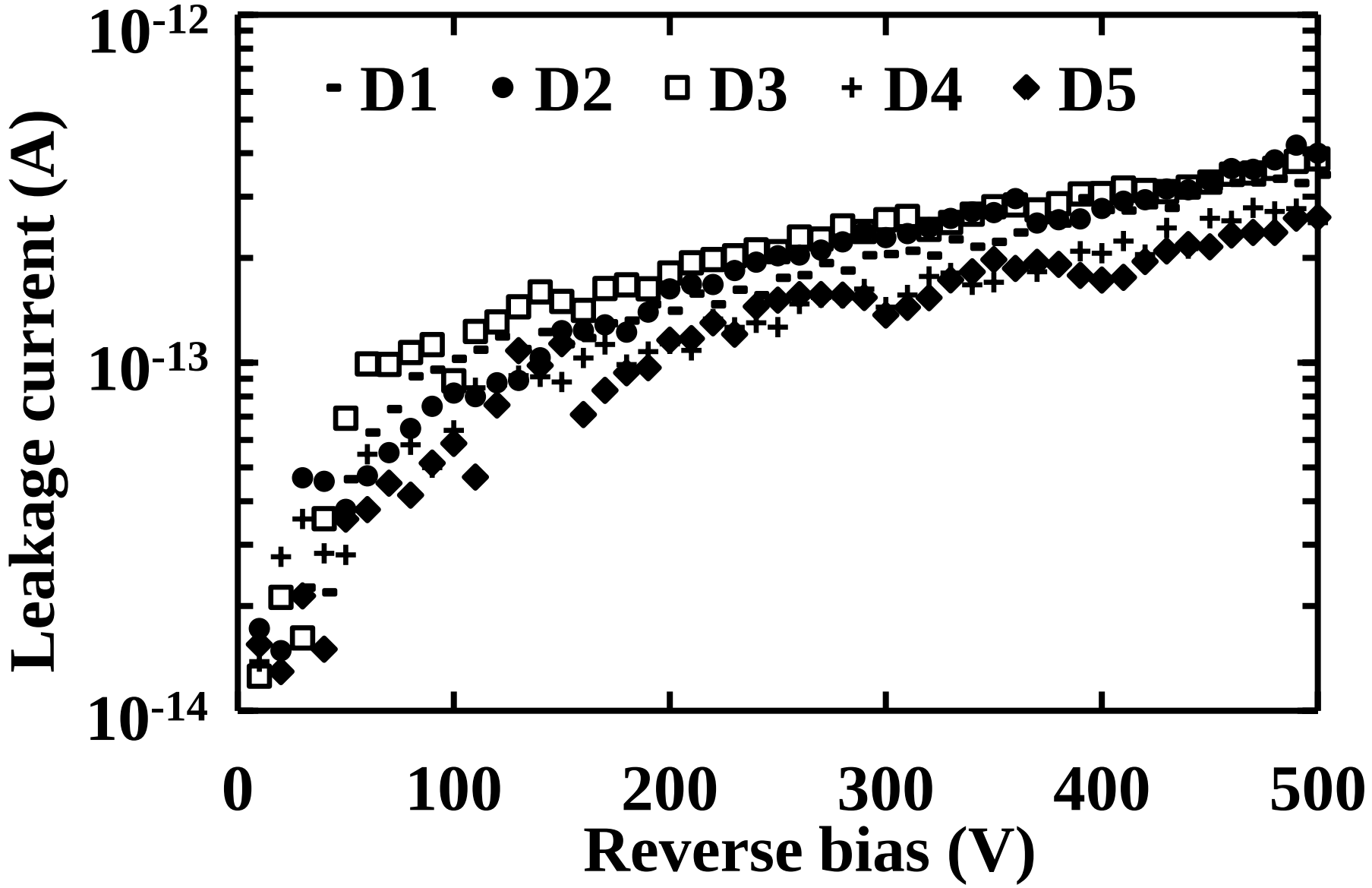
10-12
10-13
10-14
Leakage current (A)
D1
D2
D3
D4
D5
0
100
200
300
400
500
Reverse bias (V)

Figure 3

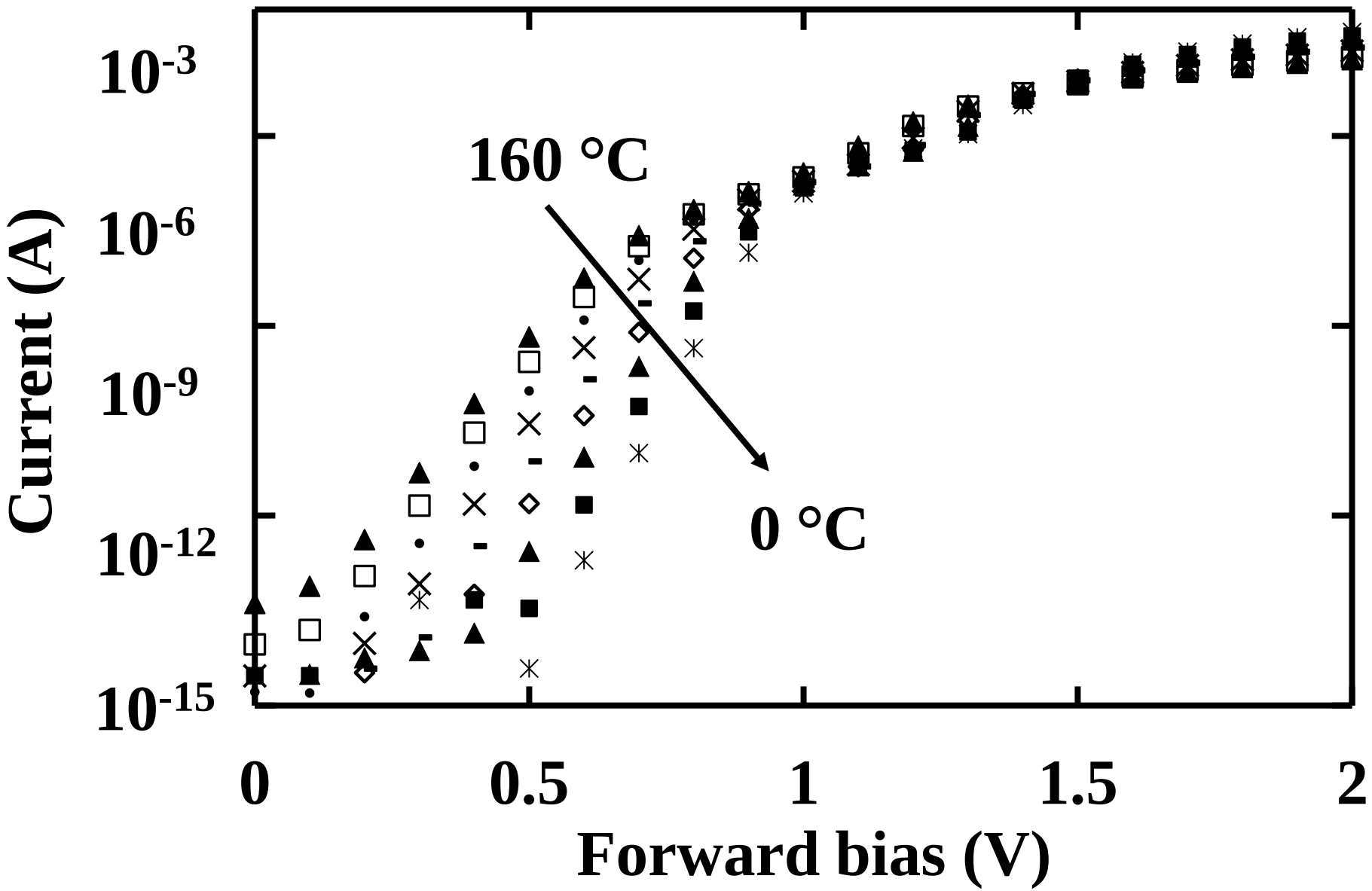
Current (A)
10-3
10-6
10-9
10-12
10-15
160 °C
0 °C
0
0.5
1
1.5
2
Forward bias (V)

Figure 4a

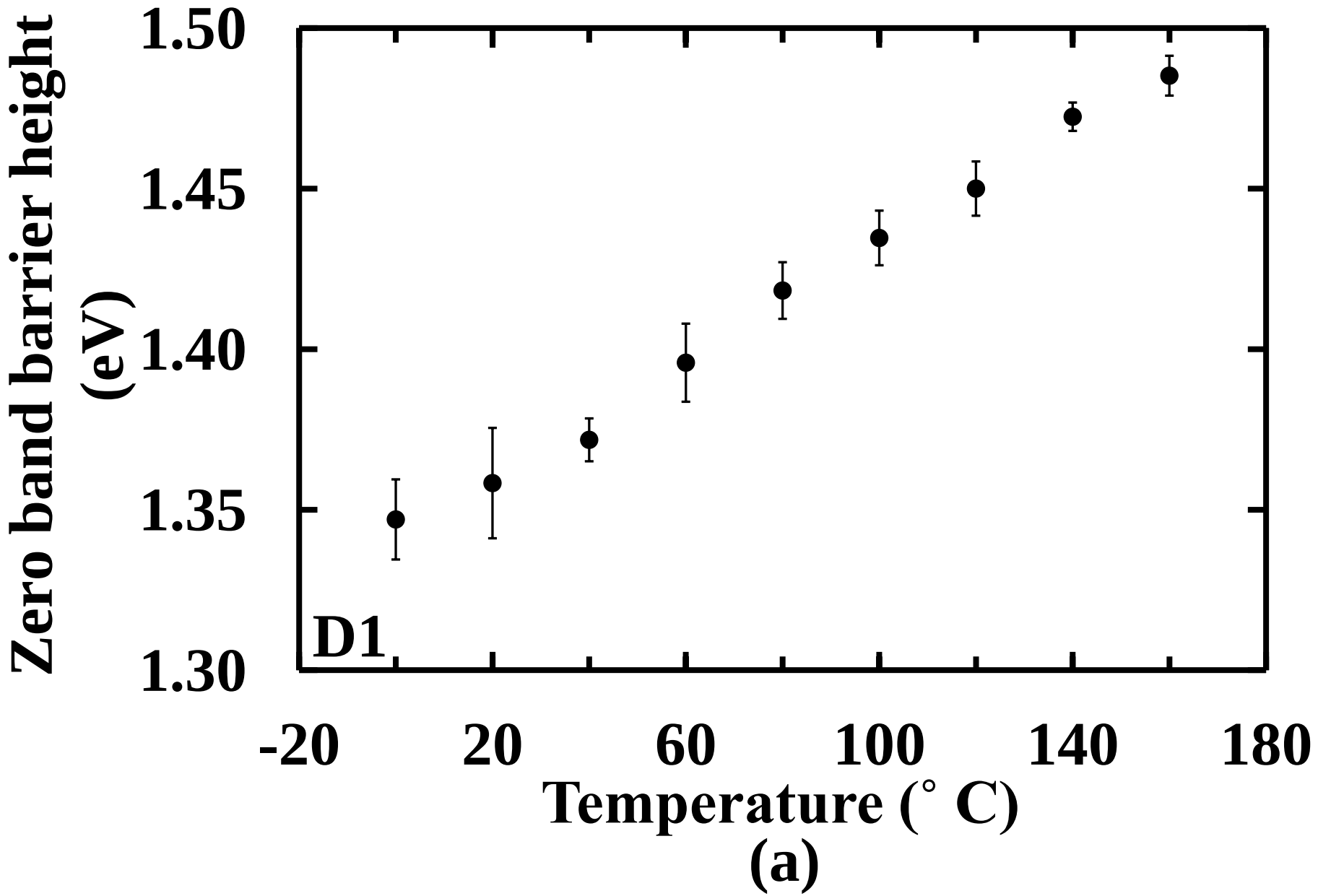
Zero band barrier height (eV)
1.50
1.45
1.40
1.35
1.30
D1
-20
20
60
100
140
180
Temperature (° C)
(a)

Figure 4b

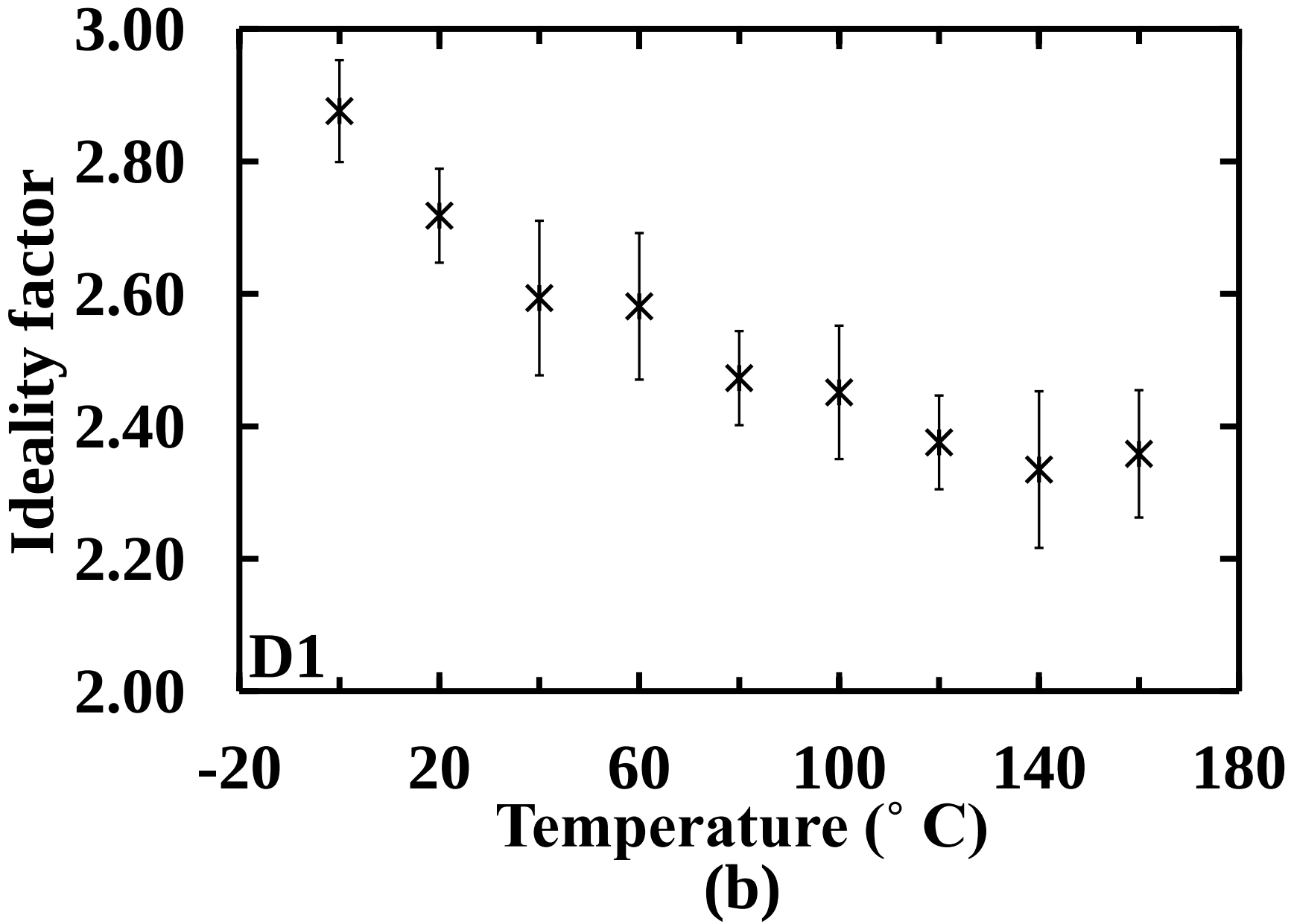
3.00
2.80
2.60
2.40
2.20
2.00
Ideality factor
D1
-20
20
60
100
140
180
Temperature (° C)
(b)

Figure 5

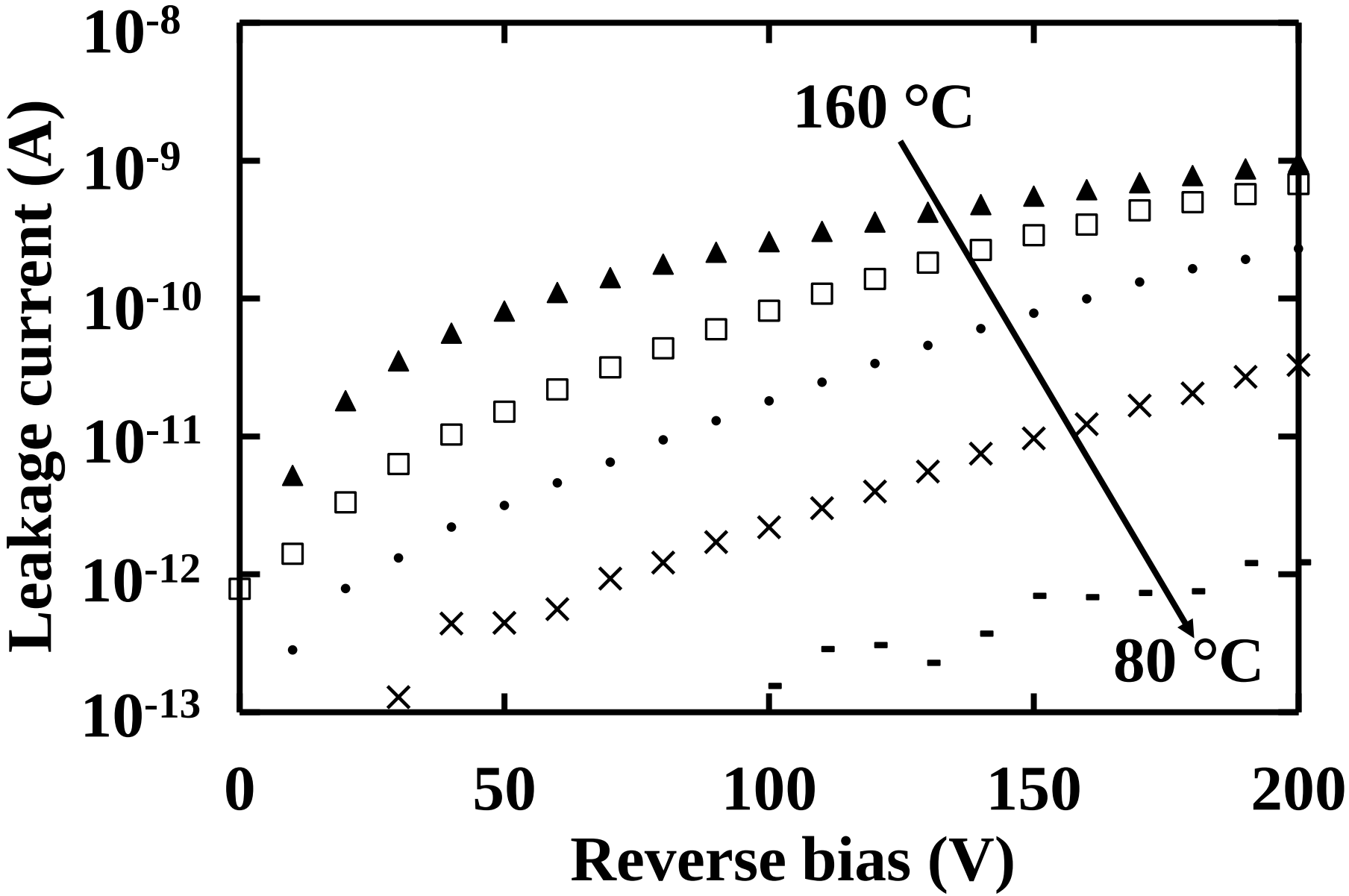
Leakage current (A)
10-8
10-9
10-10
10-11
10-12
10-13
160 °C
80 °C
0
50
100
150
200
Reverse bias (V)

Figure 6

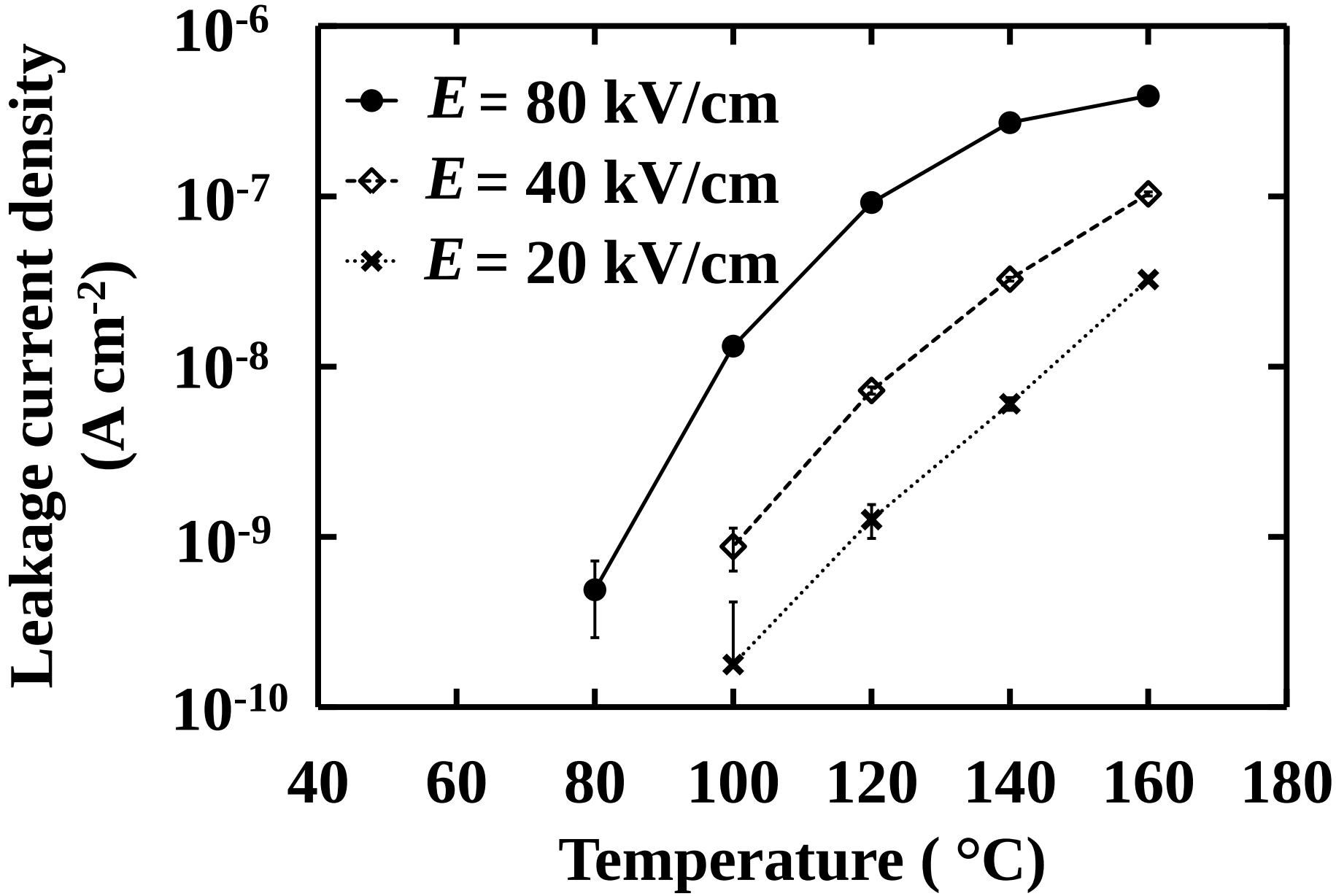
Leakage current density
(A cm-2)
10-6
10-7
10-8
10-9
10-10
E = 80 kV/cm
E = 40 kV/cm
E = 20 kV/cm
40
60
80
100
120
140
160
180
Temperature (°C)

Figure 7a

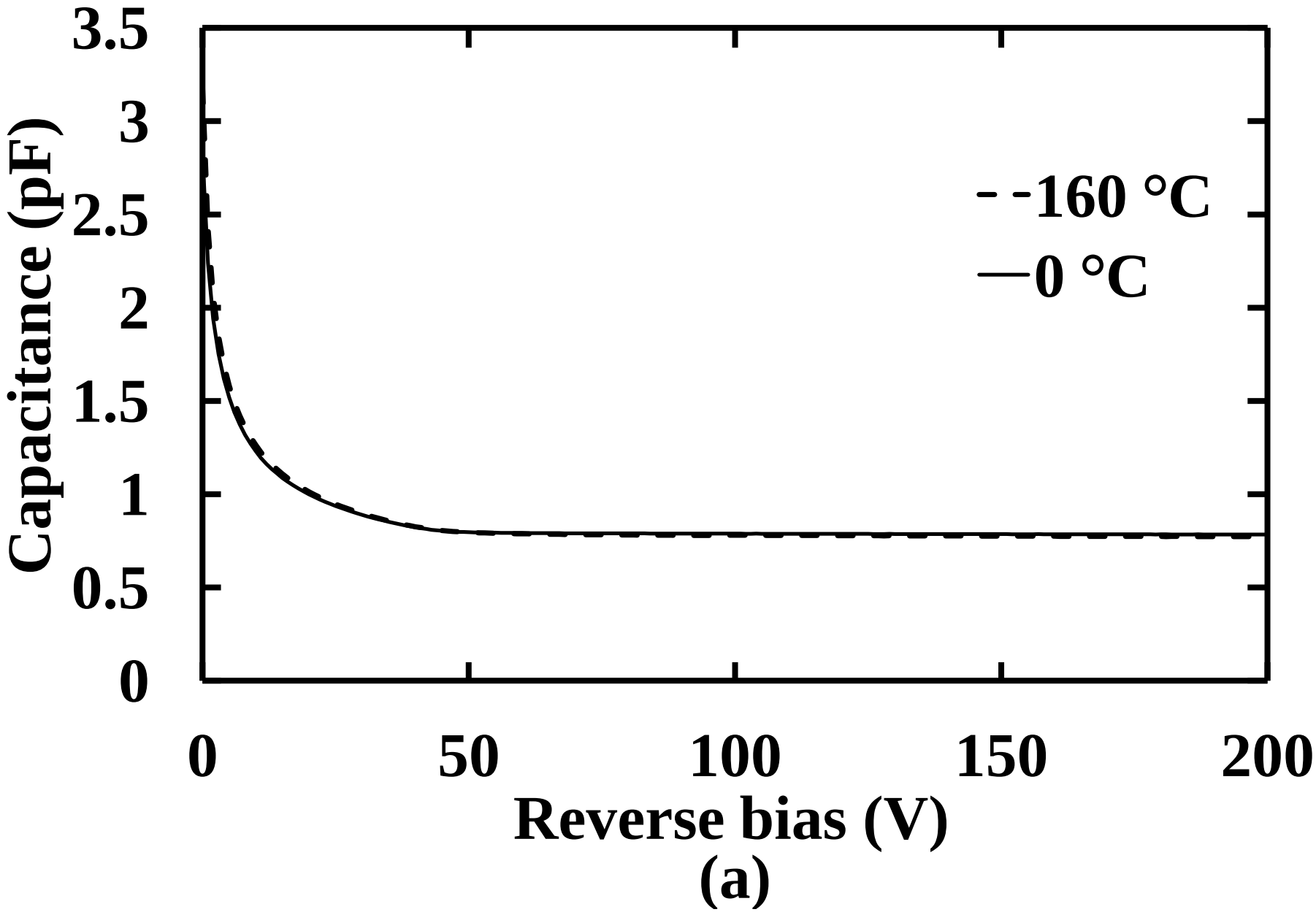
3.5
3
2.5
2
1.5
1
0.5
0
Capacitance (pF)
- -160 °C
—0 °C
0
50
100
150
200
Reverse bias (V)
(a)

Figure 7b

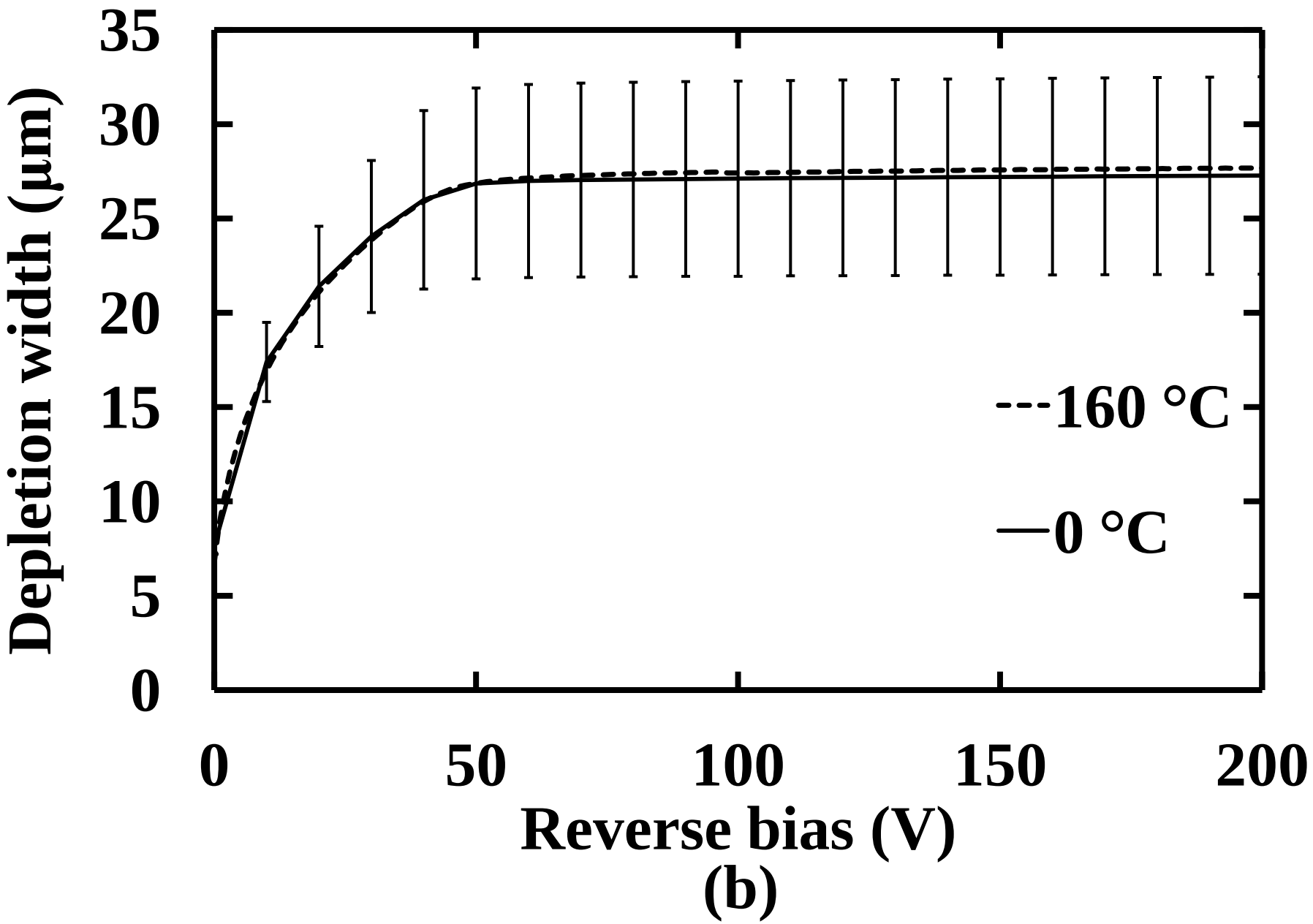
Depletion width (μm)
35
30
25
20
15
10
5
0
0
50
100
150
200
Reverse bias (V)
---160 °C
—0 °C
(b)

Figure 8

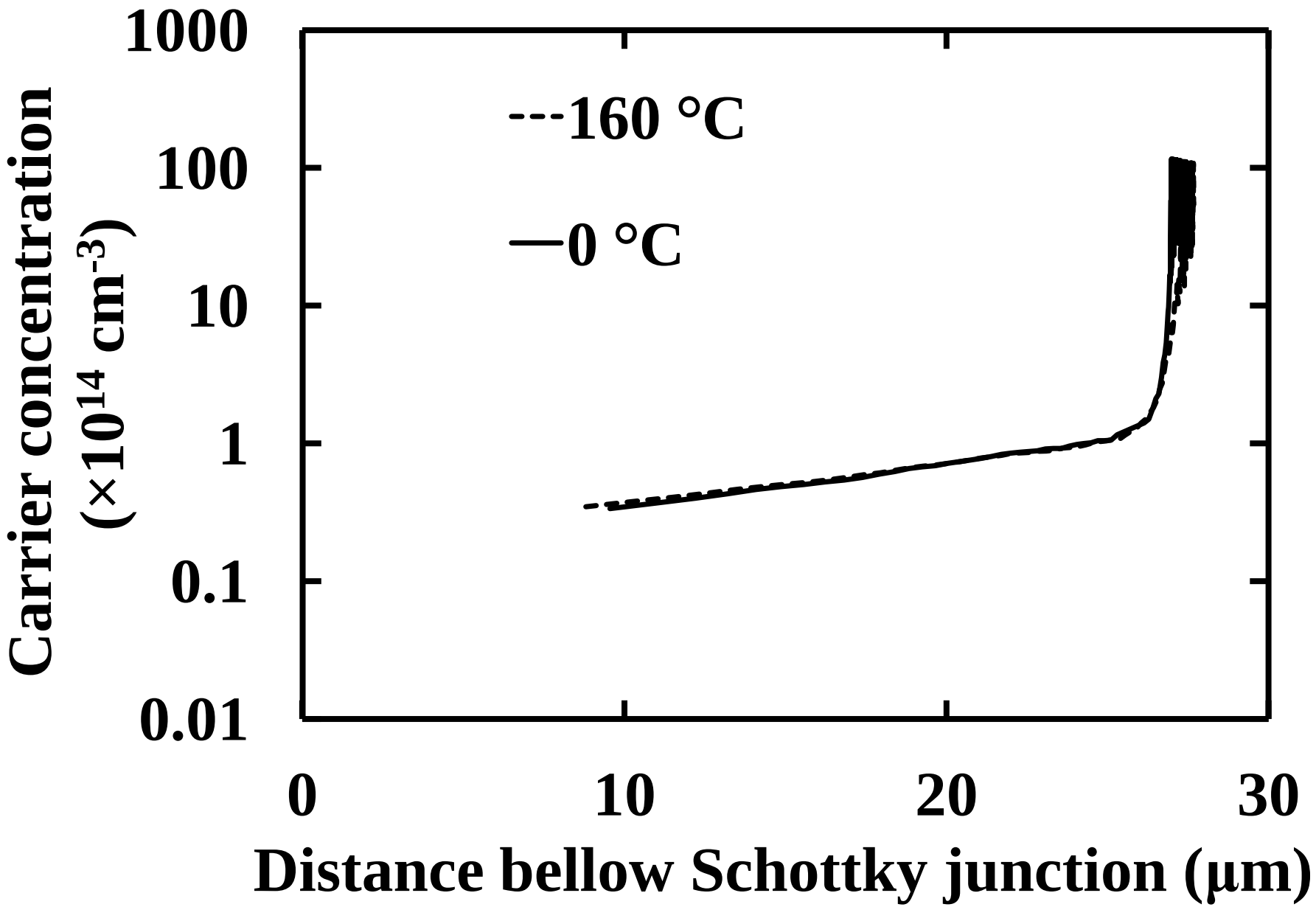
1000
100
10
1
0.1
0.01
Carrier concentration
(×10^14 cm^-3)
---160 °C
—0 °C
0
10
20
30
Distance bellow Schottky junction (μm)

Figure 9

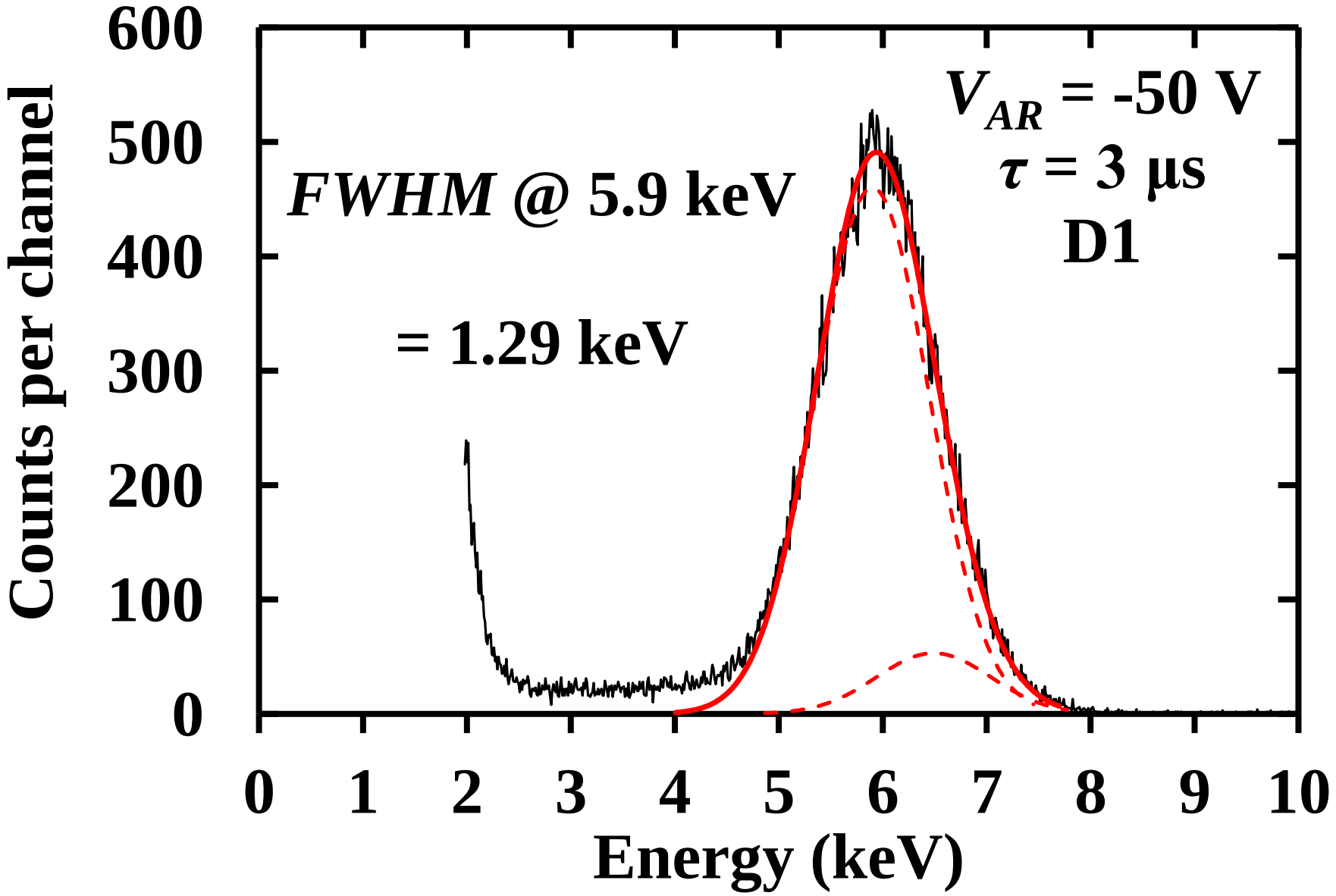
Counts per channel
600
500
400
300
200
100
0
0 1 2 3 4 5 6 7 8 9 10
Energy (keV)
V_{AR} = -50 V
τ = 3 µs
D1
FWHM @ 5.9 keV
= 1.29 keV

Figure 10

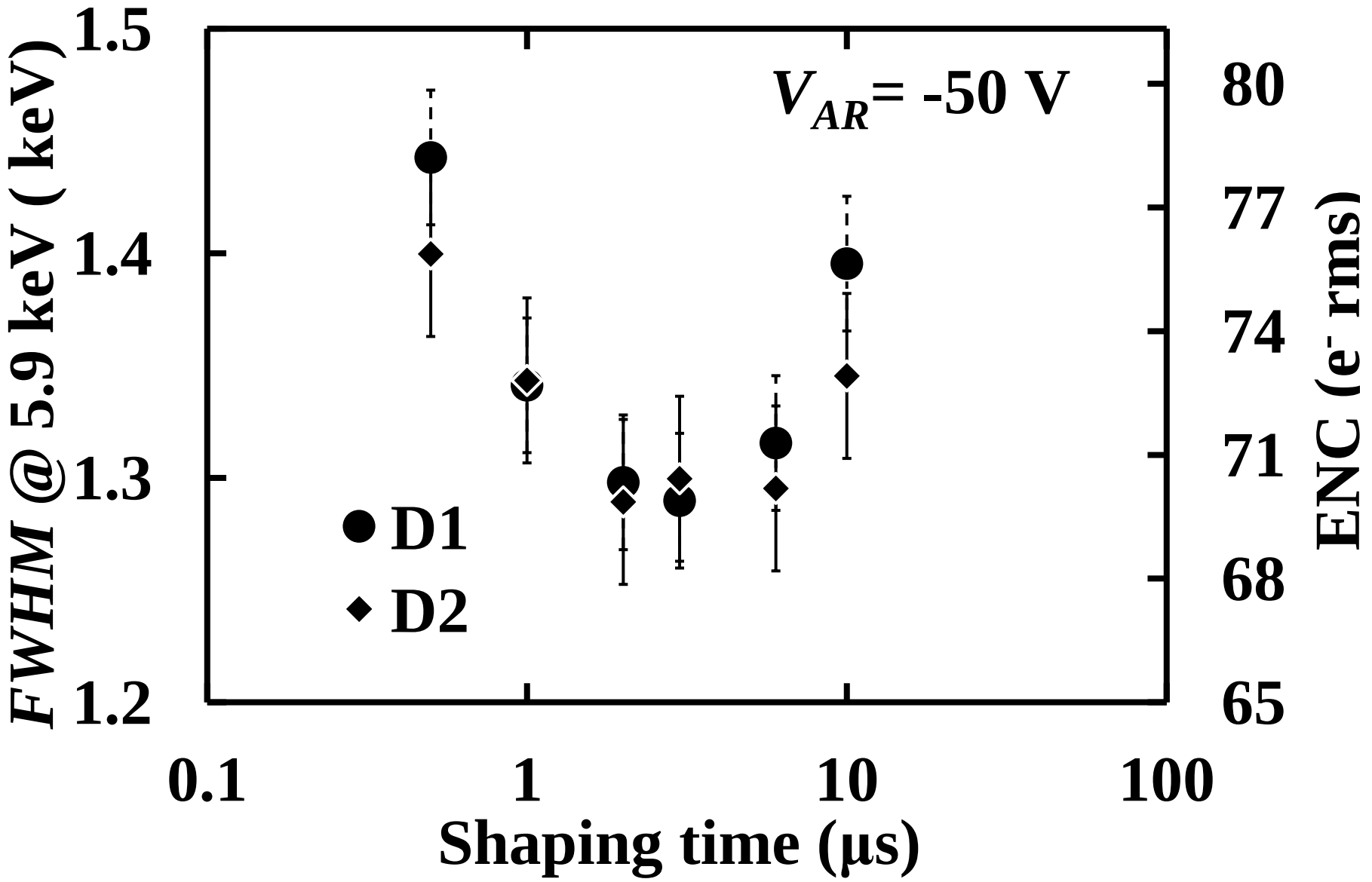
V_{AR}= -50 V
D1
D2
FWHM @ 5.9 keV (keV)
ENC (e- rms)
1.5
1.4
1.3
1.2
80
77
74
71
68
65
0.1
1
10
100
Shaping time (µs)

Figure 11a

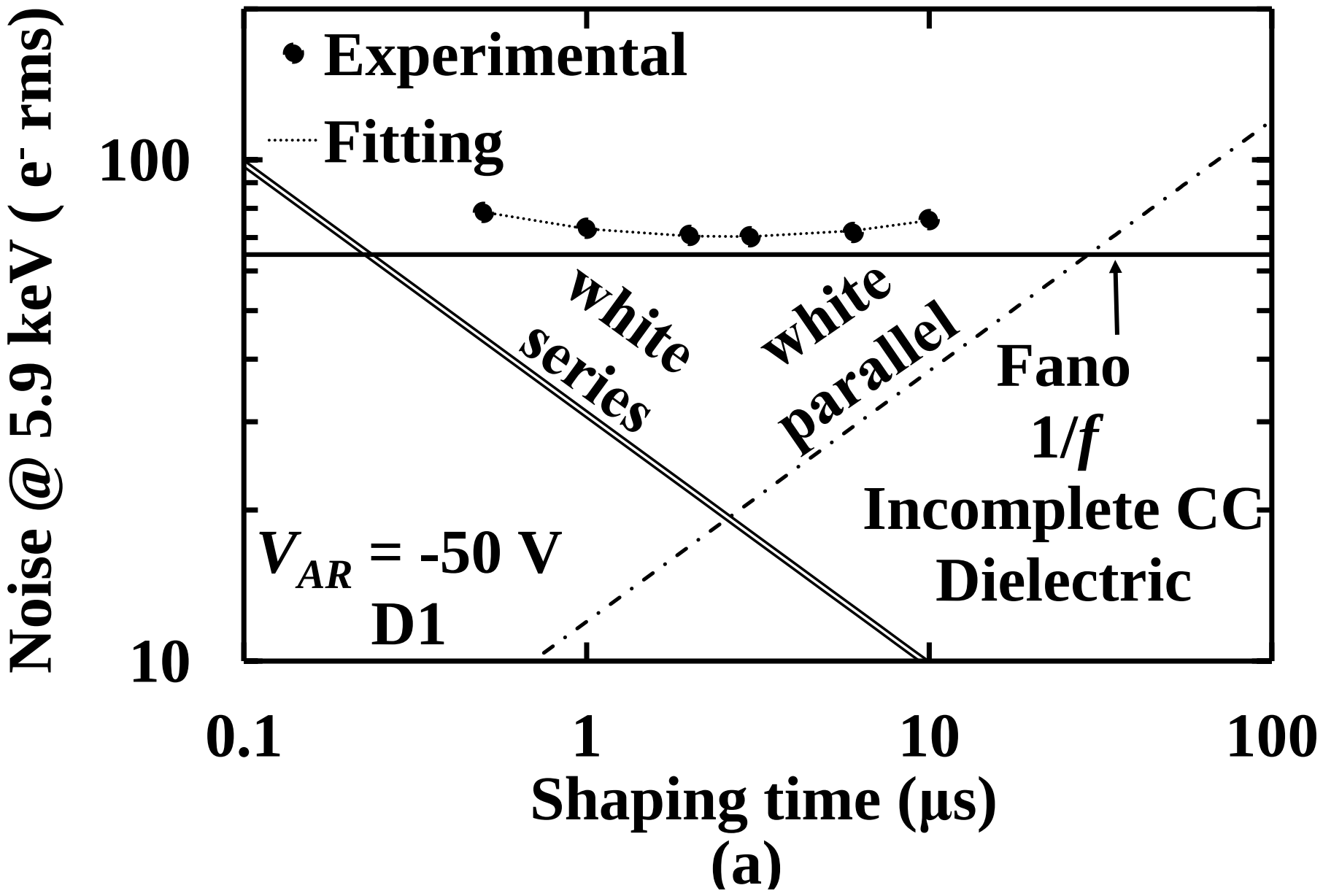
Experimental
Fitting
100
10
Noise @ 5.9 keV (e⁻ rms)
white series
white parallel
Fano
1/f
Incomplete CC
Dielectric
V_{AR} = -50 V
D1
0.1
1
10
100
Shaping time (μs)
(a)

Figure 11b

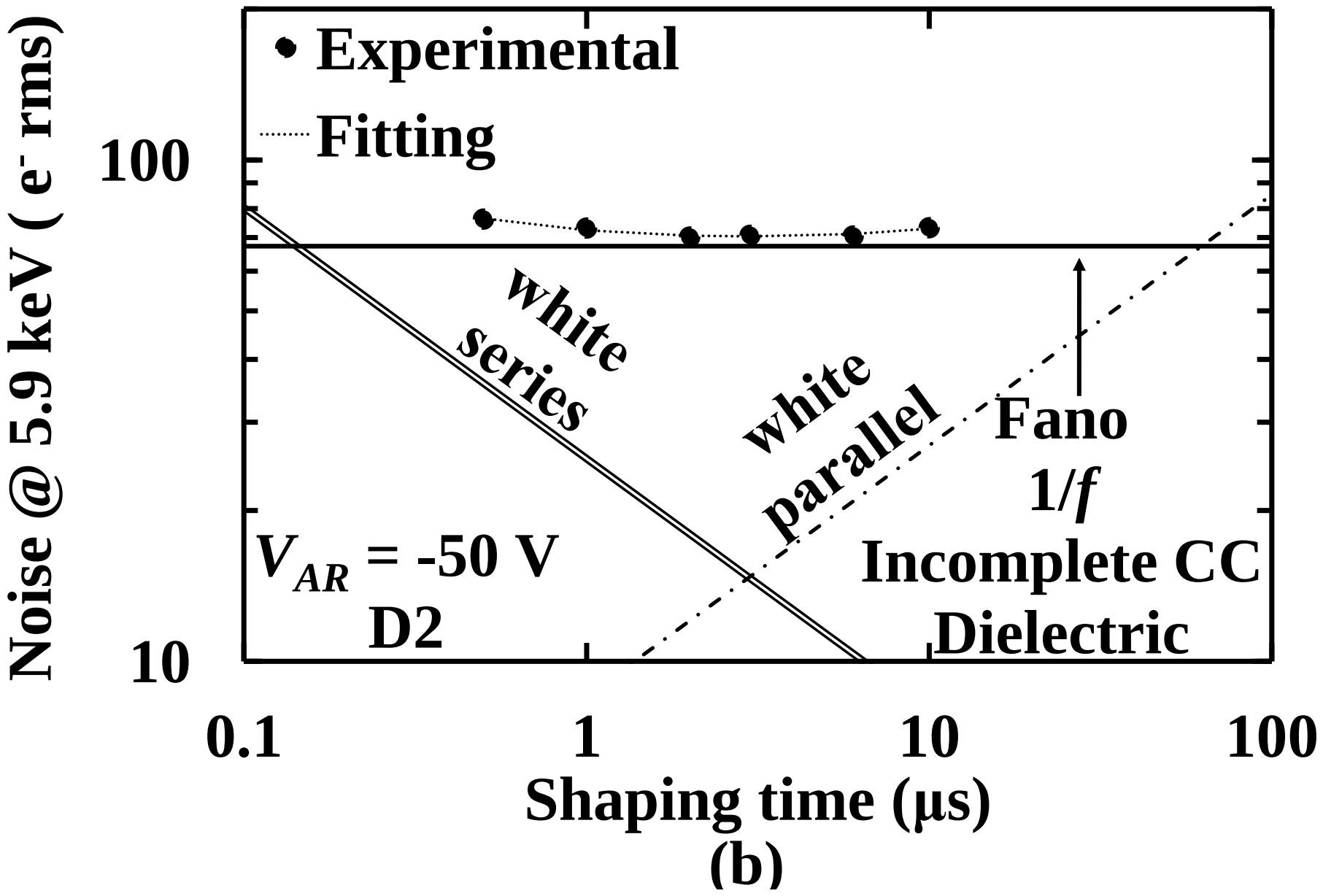
Experimental
Fitting
100
10
Noise @ 5.9 keV (e⁻ rms)
white series
white parallel
Fano
1/f
Incomplete CC
Dielectric
V_{AR} = -50 V
D2
0.1
1
10
100
Shaping time (μs)

(b)

Figure 12a

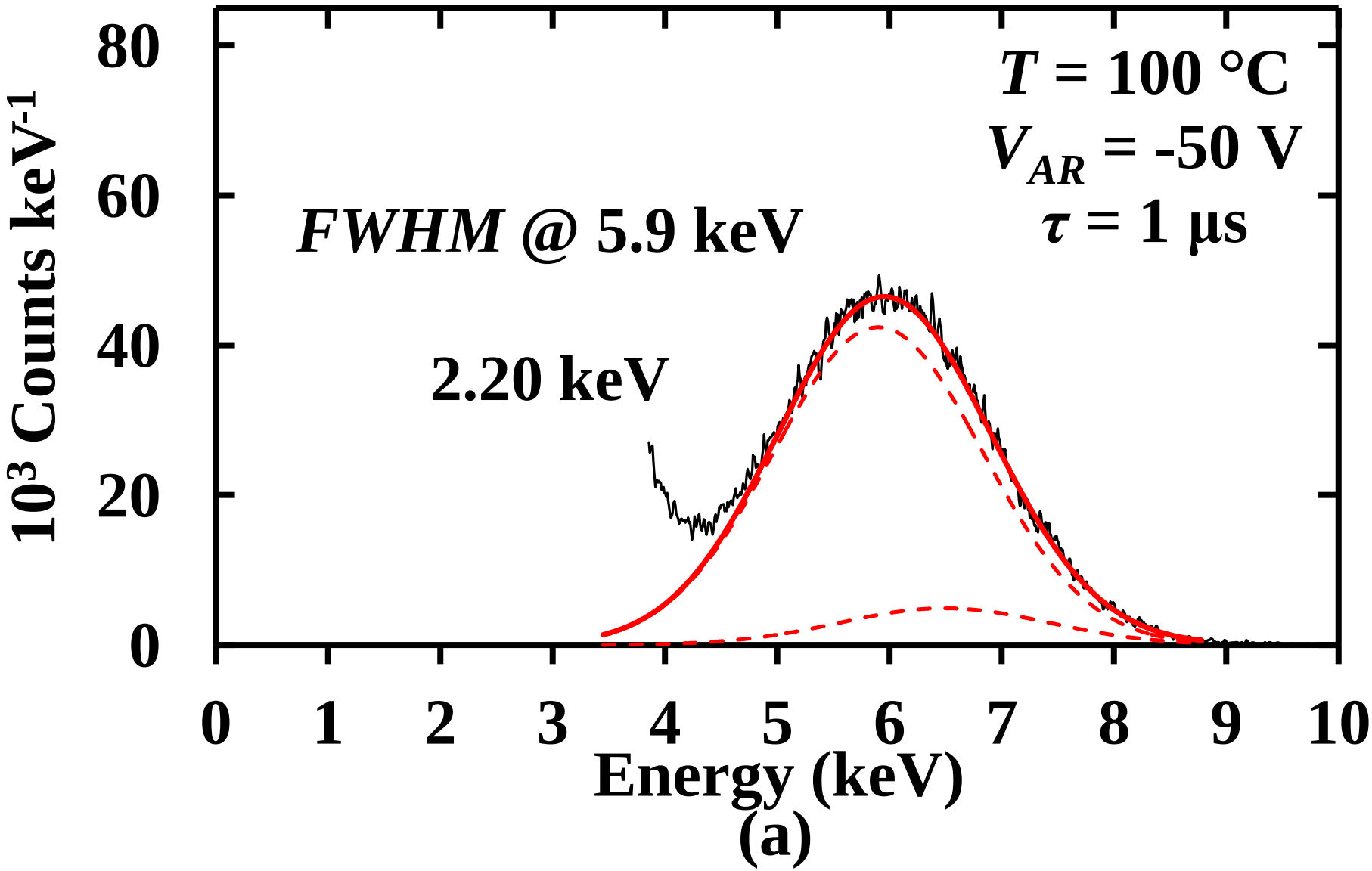
80
60
40
20
0
10^3 Counts keV^{-1}
T = 100 °C
V_{AR} = -50 V
τ = 1 µs
FWHM @ 5.9 keV
2.20 keV
0 1 2 3 4 5 6 7 8 9 10
Energy (keV)
(a)

Figure 12b

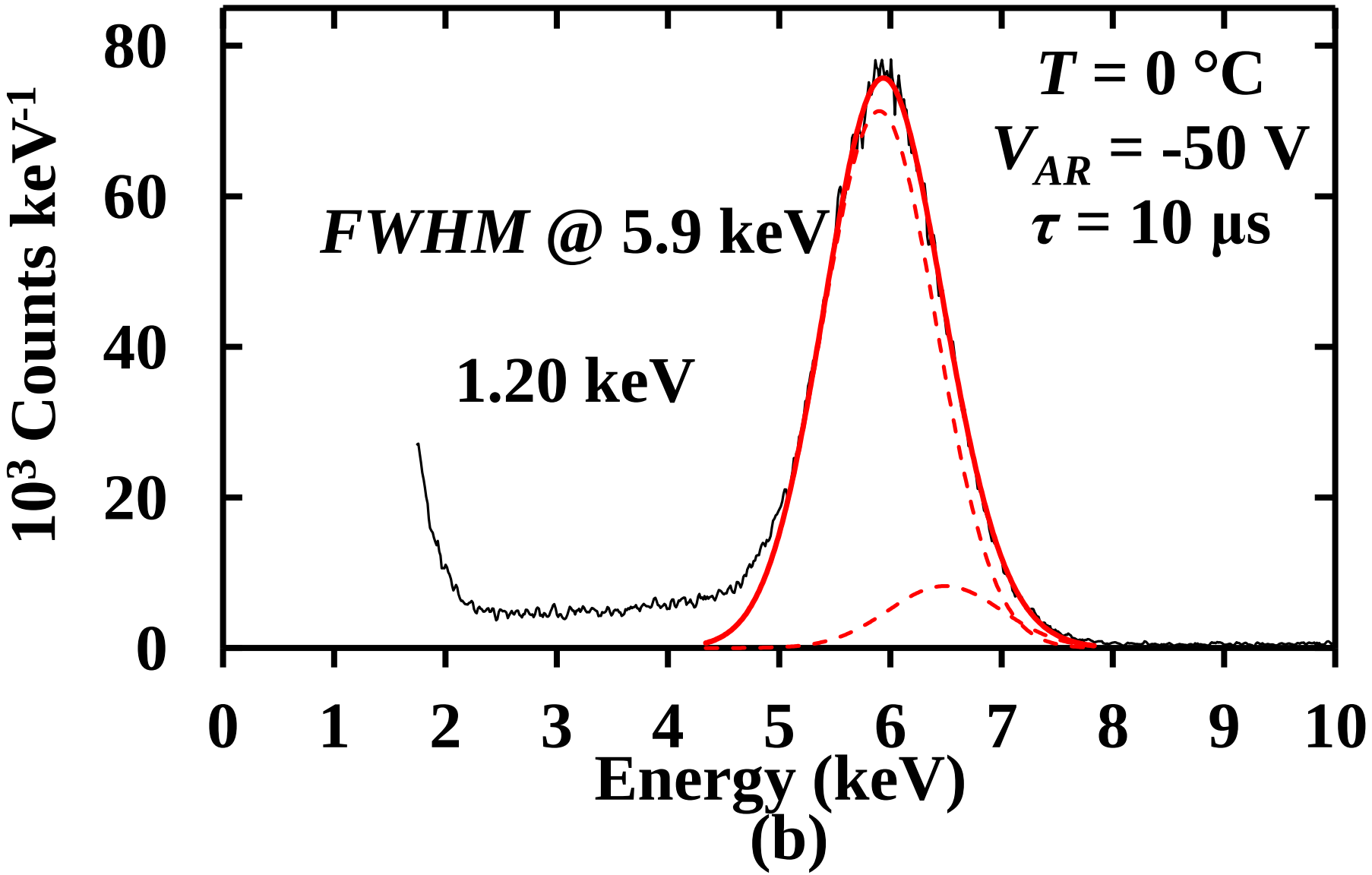
80
60
40
20
0
10^3 Counts keV-1
0 1 2 3 4 5 6 7 8 9 10
Energy (keV)
T = 0 °C
V_{AR} = -50 V
τ = 10 µs
FWHM @ 5.9 keV
1.20 keV

(b)

Figure 13

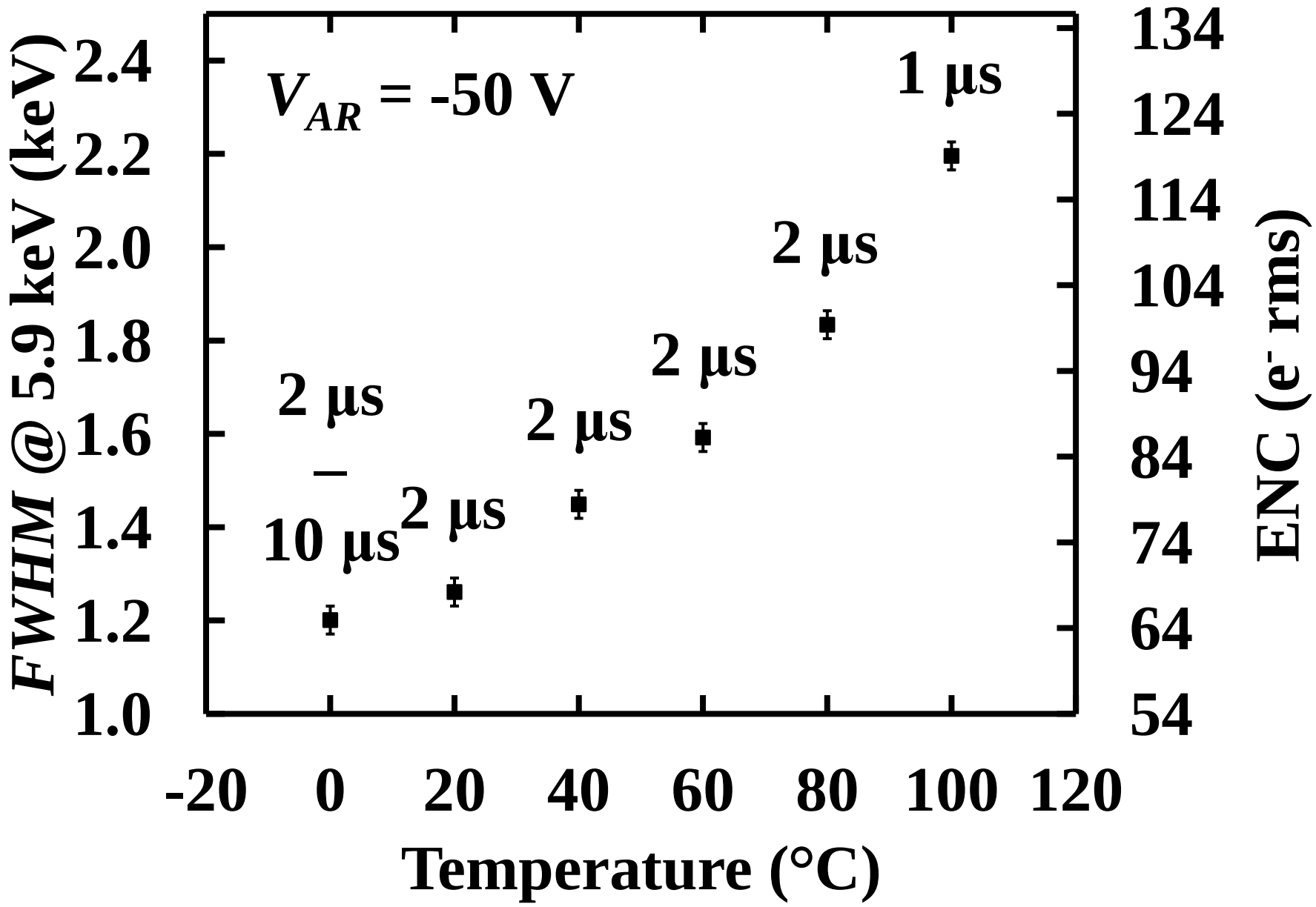
V_{AR} = -50 V
1 µs
2 µs
2 µs
2 µs
2 µs
2 µs
10 µs
FWHM @ 5.9 keV (keV)
ENC (e- rms)
Temperature (°C)
2.4
2.2
2.0
1.8
1.6
1.4
1.2
1.0
134
124
114
104
94
84
74
64
54
-20
0
20
40
60
80
100
120

Figure 14

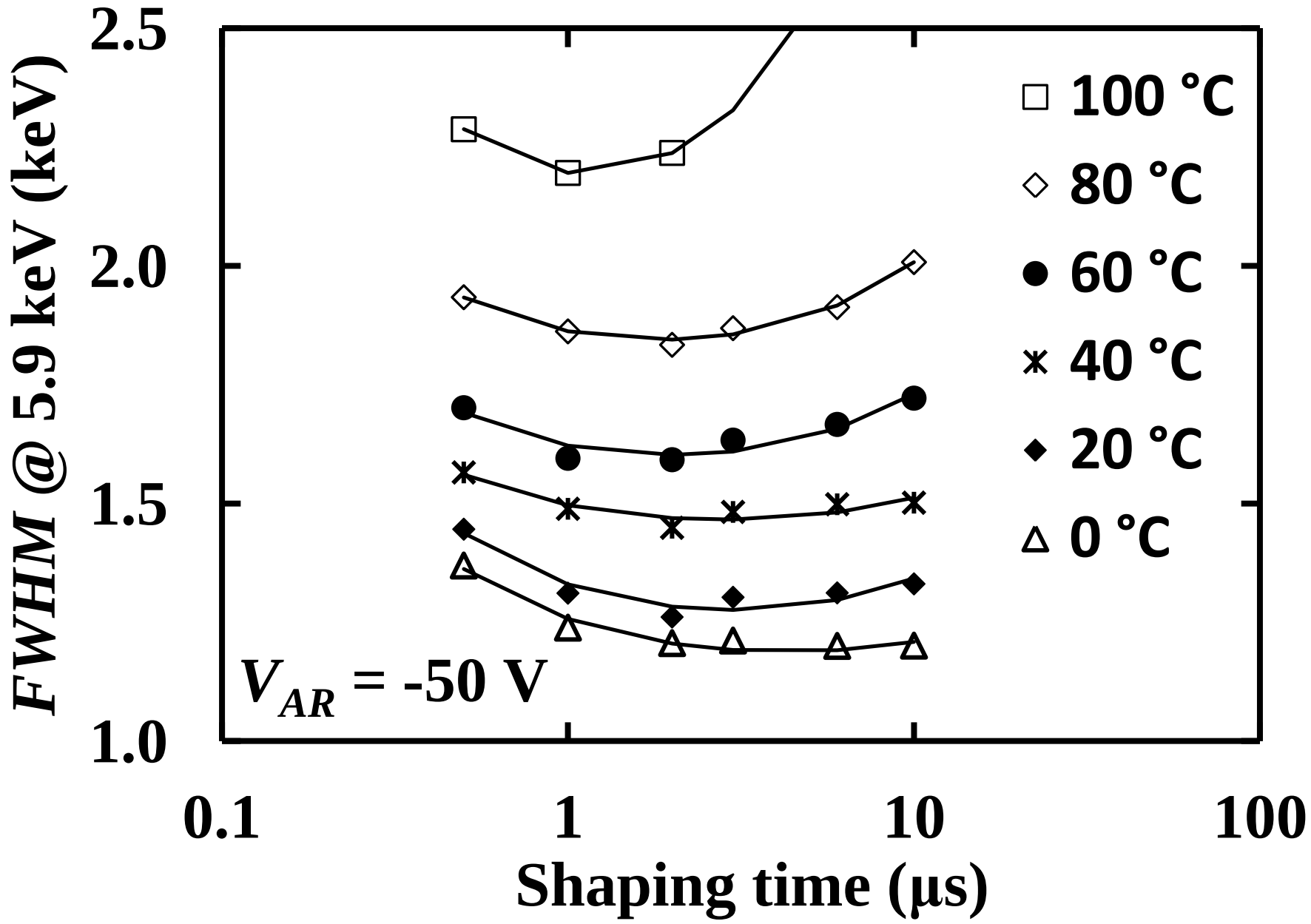
2.5
2.0
1.5
1.0
FWHM @ 5.9 keV (keV)
100 °C
80 °C
60 °C
40 °C
20 °C
0 °C
V_{AR} = -50 V
0.1
1
10
100
Shaping time (µs)

Figure 15a

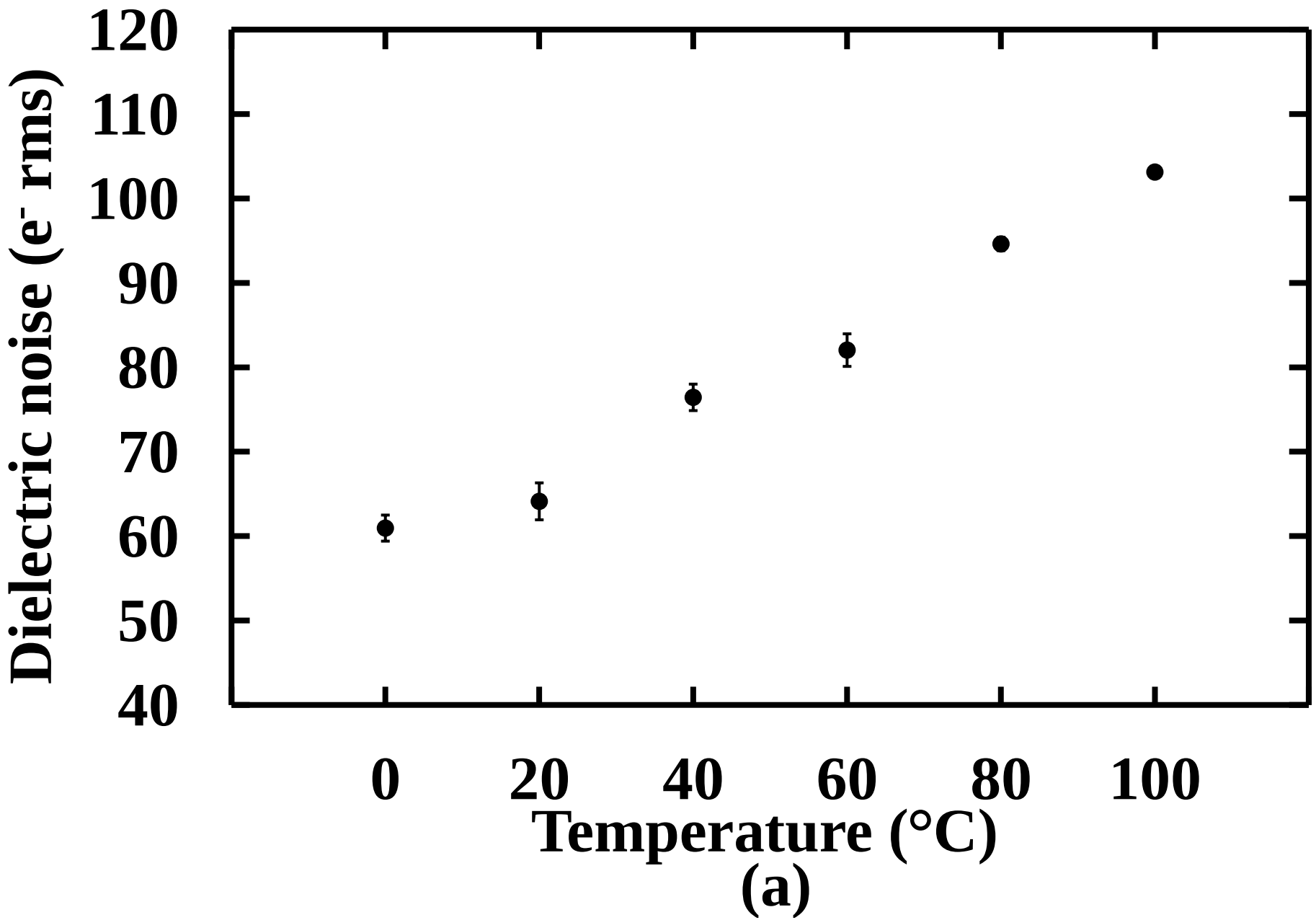
120
110
100
90
80
70
60
50
40
Dielectric noise (e- rms)
0
20
40
60
80
100
Temperature (°C)
(a)

Figure 15b

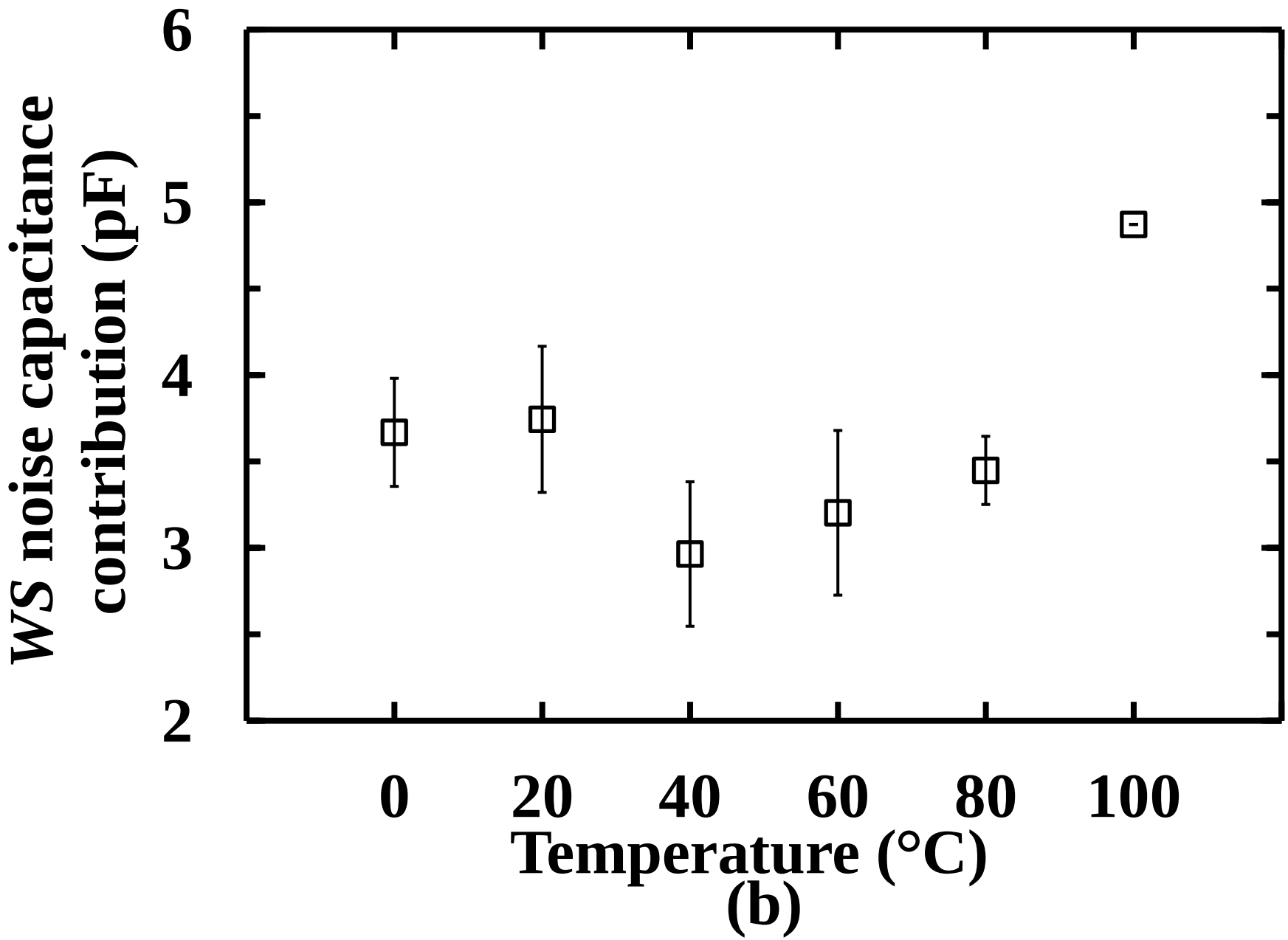
WS noise capacitance contribution (pF)
6
5
4
3
2
0
20
40
60
80
100
Temperature (°C)
(b)

Figure 15c

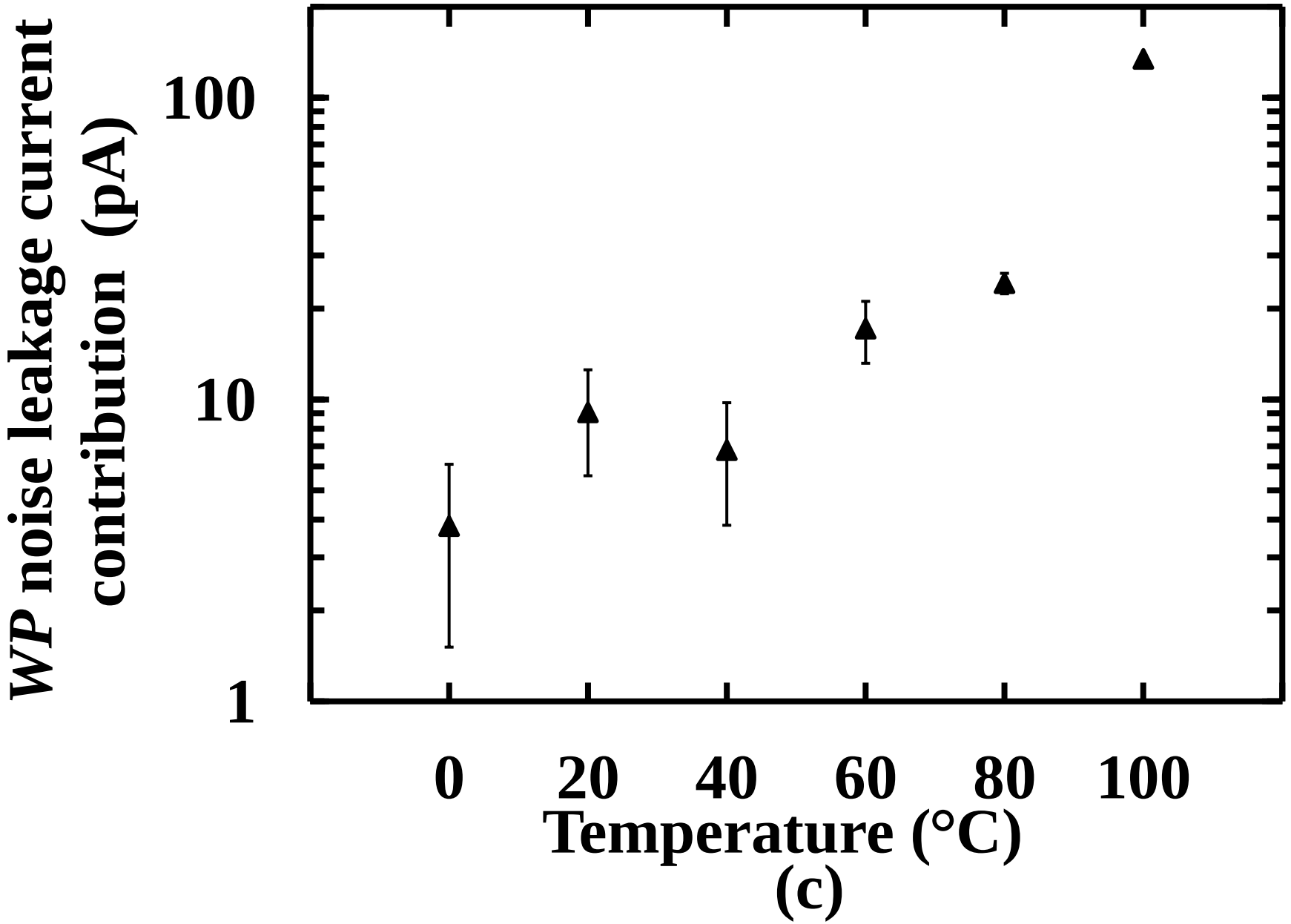
WP noise leakage current contribution (pA)
100
10
1
0
20
40
60
80
100
Temperature (°C)
(c)